The Production of Energetic Protons in Nuclei Exposed to 300 Mev Bremsstrahlung

A Thesis

Presented to the Faculty of the Graduate School of Cornell University for the Degree of

Doctor of Philosophy

By

James Collyer Keck

June 1951

James Collyer Keck was born in New York City on June 11, 1924. He attended public and private schools in New York State. In 1942, he matriculated at Cornell University. As an undergraduate he studied under a Cornell Tuition Scholarship and a New York State Scholarship. In 1944, he was drafted into the Army and assigned to the Los Alamos Laboratory as a technical assistant. After two years in service, he re-entered Cornell and in 1947 received the degree of Bachelor of Arts. Since that time he has been enrolled in the Graduate School of that institution and has served as a teaching and research assistant in physics. During 1949-50 he studied under an AEC predoctoral fellowship.

Acknowledgement

The author wishes to express his appreciation to Professor R. R. Wilson for his personal direction of this work. He is greatly indebted to Professor H. A. Bethe and to Doctors A. Silverman, J.S. Levinger, D. Walker and S. Kikuchi for helpful discussions and communication of results. The assistance and cooperation of the many students and staff members who ran the synchrotron are gratefully acknowledged.

This work was performed in part while the author was an AEC predoctoral fellow.

Table of Contents

I.	Introduction	1
II.	Apparatus	4
III.	Proton Experiments	10
IV.	Supplementary Experiments	14
V.	Discussion of Results	17
VI.	Summary and Conclusions	21
VII.	Appendices	
VIII.	Bibliography	
IX.	Figures	

The Production of Energetic Protons in Nuclei Exposed to 300 Mev Bremsstrahlung

Introduction

Early investigations of the secondary radiation from targets exposed to 300 Mev synchrotron photons indicated that numerous protons having energies of the order of 100 Mev were emitted at large angles to the beam. Various processes could account for the presence of a few energetic protons. However, the number observed was completely unanticipated and could not be readily explained by existing theories on the interaction of photons with nuclei. Since the identification of the particles was at best tentative in the early work, the need for better experiments was clear. It was the hope that such experiments would furnish some clues as to the mechanism of photon production and so permit a more precise evaluation of its role in the study of nuclear phenomena.

Concurrent with the investigation reported here similar studies were being carried out by other experimenters. D. Walker[1] used photographic plates to study protons generated by 195 Mev synchrotron radiation. Silverman and Levinthal[2] used proportional counters to detect protons in the energy range from 10 to 70 Mev produced by 320 Mev synchrotron radiation. A series of experiments which may well bear an important relation to the proton experiments are being performed by S. Kikuchi[3,4] who is studying the production of photon stars in photographic plates. The energetic protons could

be prongs of these stars.

In the present experiment various solid targets were exposed to the collimated beam from the 300 Mev Cornell synchrotron. Secondary particles coming from the targets were detected with a proportional counter telescope consisting of two NaI scintillators. Particles of different mass were distinguished by measuring their specific ionization for a fixed residual range. Electrons, mesons, protons, deuterons and heavier particles could be resolved. Accurate calibrations for the counters were obtained from the known range-energy relations.

Protons were the most numerous of the ionizing secondaries. Due to the thickness of the counters only protons above 70 Mev could be detected. The most complete data on the spectrum of the protons was obtained for production in carbon. However, limited experiments with cadmium indicate that the production process is similar in heavy elements except for the effects of scattering on the escaping protons.

The features of the proton spectrum studied were the energy and angular distributions, the Z-dependence, and the excitation function. The energy distribution falls off about as the -1.7 power of the proton energy up to about 150 Mev. Above this energy the decrease is much more rapid. The angular distribution shows a strong forward asymmetry which becomes more pronounced with increasing proton energy. The yield is nearly proportional to Z. The excitation function exhibits a threshold for the production of

105 Mev protons in the neighborhood of 200 Mev synchrotron energy.

A preliminary search for neutrons was also made. The results are consistent with approximately equal numbers of protons and neutrons.

The number of processes by which photons can produce energetic protons is quite large. In the summary we have considered some of the more obvious ones and attempted to indicate the angular and energy range in which each is most important. We conclude that most of the protons produced in the forward direction are probably of electro-magnetic origin and that the most likely number of nucleons strongly involved in the interaction is two. Theories along these lines, investigated by Levinger[5] and by Silverman and Levinthal[2], meet with partial success in describing the observations.

II Apparatus

A. General Description

In this experiment, various targets were exposed to the photon beam from the Cornell synchrotron and the spectrum of the secondary protons produced was studied with a detecting telescope consisting of two NaI scintillators. A plan drawing of the experimental arrangement is shown in Fig. 1.

To make counting with a slow phosphor like NaI possible, the beam was "expanded" to approximately 2000 μ sec. Since the magnetic field of the synchrotron varies at 30 cycles per sec., the electrons producing the photons are not monochromatic but are distributed in energy from 280 to 310 Mev[6] with an average energy of about 300 Mev. The photon beam was collimated by a 2 cm hole and had a diameter of 5 cm at the position of the external targets. The integrated beam intensity for a run was measured by the charge collected in two ionization chambers: one in front of the targets, monitor 1, and the second behind the targets, monitor 2. The chamber associated with monitor 2 was embedded in a block of lead at a depth of 1 cm. This located it approximately at the maximum of the transition curve for high energy bremsstrahlung and made it virtually insensitive to scattered radiation from collimator and slit systems. The absolute calibration of this monitor is described in Part B of this section.

A drawing of the detecting telescope is shown in Fig. 2. It employed two NaI(Tl) crystals mounted on RCA 5819 photomultipliers. The range interval in which particles were counted was defined by

setting an energy bias on the rear counter, counter 2, (Appendix I). A differential discriminator was used to obtain the pulse height distribution for the front counter, counter 1, in coincidence with the rear counter. Peaks corresponding to particles of different mass were easily distinguished; mesons, protons and deuterons of the same residual range have specific ionizations in the ratio of .4 ; 1 ; 1.8 respectively. The total weight of material in front of the rear counter determined the minimum range of a particle which could be detected. For mesons, protons, and deutrons this range corresponded to energies of 25, 55, and 70 Mev. The system was essentially self-calibrating. A rough preliminary comparison with the pulses produced by 2.6 Mev. thorium γ -rays enabled one to identify the peaks corresponding to different particles. Once this identification was made, a very accurate calibration could be obtained from the known range-energy relations.(7) Details of the method are given in Part C of this section.

A block diagram of the associated electronic equipment is shown in Fig. 3. The amplifiers had an overall gain of 40 and a rise time of about .1 μ sec. Coincidence gates were delay-line timed and of 1 μ sec. duration. The system was clamped except for a 5 millisec. interval bracketing the beam pulse. The data recorded were (1) the singles rate for each counter, (2) the coincidence rate, (3) the delayed coincidence (accidental) rate, (4) the pulse height distribution in either counter, alone or in coincidence with the other.

The most serious limitation on the precision of the experiment arose from the stability required in the high voltage set for the photomultipliers. The reason for this is that the range interval defined by the rear counter and hence the counting rate of the detector is extremely sensitive to the gain of the multipliers. In particular, if we wish to obtain 10% stability in the counting rate, the high voltage must be stable to .5%. Even though the high voltage was battery regulated, fluctuations of this magnitude could occur under adverse conditions and for this reason, counting was in general limited to 10% statistical accuracy and runs were repeated at least twice.

B. Absolute Beam Intensity

The absolute beam intensity has been measured in two different ways. The first measurement was made by J. Dewire with the Cornell pair spectrometer.(6) The second measurement was made by R. Littauer who determined the total energy in the beam from a measurement of the shower curve in aluminum. The monitor 2, described above, was calibrated by both methods. The results are given in Table I.

Table I

Synchrotron Energy 305 Mev.

	Q* Effective Quanta	Charge on Monitor 2, I Coulombs	Q/I Eff. Quanta/Coul.
Spectrometer	$2.6_8 \times 10^{6}$	$2.6_7 \times 10^{-10}$	1.00×10^{16}
Shower Curve	4.6×10^{6}	$4.4_5 \times 10^{-8}$	1.03×10^{16}

* The number of "effective quanta", Q, is defined as the integrated energy in the bremsstrahlung spectrum divided by maximum photon energy.

A comparison of the results shows agreement within 3%. The measurements are as yet somewhat preliminary and an accuracy of about 10% is estimated.

C. Calibration of Counters

An energy calibration for a counter was built up in the following manner: First, a rough number-bias curve was run for the 2.6 Mev. thorium γ -ray and the approximate end point determined. Next, the counter was put in coincidence with a counter behind it and a number-bias curve obtained for fast electrons generated by the synchrotron beam stiking a lead target. The results of this procedure are typified by the curves shown in Fig.4. The figure on the graph shows schematically the geometry with which the run was made. The shaded crystal, Counter I, is the one for which pulse height distribution is given. The dashed curve was obtained for the thorium γ -rays. The family of solid curves were obtained for electrons, each curve corresponding to a different voltage setting for the multiplier.

The differential number-bias curve for electrons is not Gaussian but has a tail on the high energy side and a plateau on the low energy side. The tail is to be expected since all the processes which contribute to the straggling of the electrons tend to increase the energy loss. The plateau is interpreted as due to pairs produced in the back layers of th crystal by photons. These features serve to point up the fact that the ionization produced by an electron in traversing the counter is not a well-defined quantity. For our present purposes, we assume the most probable energy lost

by an electron traversing the crystal is about 10% greater than that which would be lost by a minimum ionizing proton* . We thus obtain 4.7 Mev as the most probable energy lost in Counter 1. The agreement with the energy calibration obtained from the estimated thorium end point (indicated by the arrow on the abscissa) is better than can be justified. The widths of the electron peaks provide us with a rough estimate of the resolution of the counters. On this basis, we can reasonably expect something better than ± 15%. Subsequent observations on protons confirm this view.

The last step in the calibration was to obtain a number-bias curve for protons. The procedure differed somewhat for the front and rear counters. A typical run for the rear counter is shown in Fig. 5. The solid curve was calculated assuming the counting rate to be strictly proportional to the range interval defined by a given bias setting. (Appendix I). The dashed curve was calculated taking into account the proton spectrum and an estimated resolution of 10%. Fitting the curves to the data gives an accurate point on the calibration curve corresponding to the energy lost by a proton of range equal to the thickness of the crystal. Using this calibration point we have calculated the pulse height corresponding to a minimum ionizing proton. The value is indicated in Fig. 5, along with the observed electron pulse height. There is good agreement. The counting arrangement used in this calibration did not discriminate against deuterons or π^--mesons which produce stars. The good

* Minimum ionization for a proton was taken to be 1.65 Mev/g/cm^2 in Al.

fit of the theoretical curve is some evidence that these particles must be present only in small numbers. Better evidence is presented below.

For the front counter the proton calibration was carried out as follows: The range of the counted particles was defined by the rear counter and the pulse height distribution observed for the front counter. A typical run is shown in Fig.6. The two distributions correspond to different residual ranges. The curves indicate the expected pulse height distribution corrected for resolution and energy straggling. They were normalized to fit the experimental data at the points indicated by stars. The arrows along the abscissa indicate the expected locations of the half value points. The brackets around the arrows show the energy spread due only to the finite range interval in which the particles could stop. Also indicated on the abscissa are the expected pulse height due to a minimum proton and the observed electron pulse height. The ratio of mesons to protons was extrapolated from a statistically better measurement which is discussed later in this paper. It should be pointed out that deuterons could have been quite easily resolved had they been present with a frequency greater than about 10% of the proton frequency.

To summarize, we believe that the two crystal telescope described above can be reliably calibrated and that by using such a telescope it is possible to distinguish electrons, mesons, protons, and heavier particles with some degree of certainty.

III Proton Experiments

A. Energy Spectrum

The differential range spectrum for protons emitted at 67.5° from carbon and cadmium targets was obtained by measuring their absorption in copper ($\sum_1$, in Fig.1). The target angle, Φ , was 135°. The distance, d, from the targets to the rear counter was 20 cm., giving an angular aperture of ± 6°. The range interval defined by the rear counter was 2.6 g/cm^2 NaI. The target thickness was increased with increasing range in order to keep up the counting rate. Runs with different target thickness were overlapped to check that the number of protons was proportional to the target thickness. Backgrounds were negligible in all cases; in general there were no counts recorded at all.

The differential energy spectrum was obtained from the differential range spectrum by dividing by the value of $\frac{dE}{dR}$ appropriate for the mean range. The results are plotted in Fig. 7. as a function of the energy corresponding to the mean range. The height of the rectangle around the experimental points gives the statistical error and the width gives the total energy spread due to energy loss in the target and the finite range interval in which the particles were stopped. The maximum likely error in themeasurement of the absolute cross-section is ± 25%.

We have also plotted in Fig.7 some data on the absorption in lead which was obtained as a by-product of an experiment on neutrons described below.

In these experiments the neutrons were identified by their characteristic absorption in lead; at small absorber thicknesses the counts recorded were mostly protons. (Fig.12). The data were normalized so that the 110 Mev point should lie on a smooth curve through the copper points. Only a single counter was used in this experiment, hence the discrimination was on the basis of pulse height alone. However, since an 80 Mev pulse was required in a counter 93 Mev thick for protons, the discrimination against other particles should have been good.

A number of corrections have been investigated. These include: (1) corrections necessary for finite energy resolution and energy loss in the targets; (2) distortion of the range spectrum due to the finite angular aperture; (3) loss of particles and distortions due to multiple Coulomb scattering; (4) effects of range and energy straggling; (5) loss of particles due to nuclear absorption and scattering. Only the last correction is appreciable. In this case it is a reasonable approximation to assume that all particles which suffer a nuclear encounter are lost. For proton energies less than 150 Mev. even this correction is small. At energies greater than 150 Mev., the correction changes the slopes of the curves in Fig. 7 from -7 to -6 for carbon and from -9 to -7 for cadmium.

B. Angular Dependence

The angular distribution for protons from carbon for energies of 100, 130, and 175 Mev is shown in Fig. 8. The curves are norm-

alised to unity at 67.5°. For angles ≤ 90°, the target angle (ϕ in Fig. 1) was 135°; for angles ≥ 90°, the target angle was 45°. The distance, d, from the target to the counter was increased to obtain better angular resolution as the angle between the beam and the counters was decreased. The height of the rectangle in Fig. 8 gives the statistical error and the width gives the total angular aperture including finite extension of the target.

An angular distribution was also attempted for cadmium. The data are given in Fig. 9. A large background of scattered electrons was encountered in the forward direction which severely limited the experiment. The data are sufficient to show that the distribution for cadmium is similar to that for carbon.

In so far as the relative values of the yield are concerned, there is only one correction that might be made. This arises because protons emitted at different angles suffer a different energy loss in the target so that their mean energy varies slightly with angle of observation. The maximum error occurs at 90° where it amounts to -2% in the energy.

C. Total Cross-sections.

The angular distributions for carbon have been plotted as a function of cos Θ and integrated graphically to obtain total cross-sections at 100, 130, and 175 Mev. The results are given in Table II.

Table II

Proton Energy E Mev	$\frac{d\sigma(E)}{dE}/4\pi \quad \frac{d\sigma(E, 67.5°)}{dE\, d\Omega}$
100	.65 ± .07
130	.69 ± .07
175	.88 ± .09

It can be seen that the total cross-section is very nearly proportional to the differential cross-section at 67.5°, so that the differential energy spectrum given in Fig. 7 also represents reasonably well the variation of the total cross-section with energy.

D. Z-Dependence

The proton yield per nucleus for various targets was measured and is plotted as a function of Z in Fig. 10. The target thicknesses were chosen to have approximately equal stopping power for protons. A correction was made for absorption of the synchrotron beam in the heavy targets. This amounted to about + 20% for cadmium and lead and + 10% for copper. In making the correction it was assumed that if a photon interacted at all it was effectively removed from the beam as far as the production of 130 MEV protons was concerned.

E. Excitation Function

An excitation function for the production of 105 Mev protons at 30°(Fig.11) was constructed from data obtained from three sources.

An early measurement made by Keck, Stearns, and Wilson (unpublished) gave points for synchrotron energies of 155, 180, and 220 Mev. These points are plotted as squares in Fig. 11. The geometry for the experiment is shown in the figure on the graph. A single NaI scintillator employing a 4 cm diameter by 5 cm high crystal was used. The situation is somewhat complicated because the protons

traversed the crystal in a direction perpendicular to its axis. However, this has only a small effect on the relative values. Discrimination against mesons was on the basis of pulse height only. The absolute detection threshold for mesons occurs at a synchrotron energy of 180 Mev. At 220 Mev the meson yield is still small compared with the number of observed counts and since the counter was biased at 70 Mev, a meson would have to produce a large star to be counted at all. Under these conditions the number of counts due to mesons should have been negligible.

Unfortunately the data of Keck, Stearns, and Wilson can not be used to calculate an absolute cross-section. They were therefore normalized to the results of Walker [1] at 195 Mev synchrotron energy in plotting Fig.11. The value of Walker's point realtive to the 300Mev point should be reliable within the statistical error since Walker used the same monitors as were employed in the present experiment.

IV Supplementary Experiments

A. High Energy Neutrons

Since the existence of high energy neutrons follows almost as a corollary from the existence of high energy protons, a preliminary search for such neutrons was made. The neutronscounter consisted of a liquid scintillator (employing terphenyl [6] dissolved in xylene) surrounded by a 2" thick lead shield. The active volume of the counter was 4.4 cm in diameter by 7.6 cm long. These dimensions correspond to proton ranges of 70 and 58 Mev respectiv-

ely. The counter was calibrated in the same way as the NaI counters described above. The ratio of the proton pulse height to the electron pulse height was 5.4. The expected ratio was 6. The agreement is sufficient to establish a reasonable degree of proportionality for the liquid scintillator.

Neutrons were identified by observing their characteristic absorption in lead. A typical absorption curve is shown in Fig. 12. The diagram in the corner gives schematically the geometry for the run. The target was 1" of carbon at 135°. The angle of observation was 67.5°. The solid lines through the points at large absorber thickness have been drawn with a slope corresponding to the geometric mean free path for lead, 5.8". It can be seen that for an absorber thickness > 2" most of the counts may be attributed to neutrons. The dashed curves represent the expected number of proton counts added to the neutron counts. The additional counts at the lowest bias may be attributed to electron-photon cascades.

In Table III we have given the number of neutron counts extrapolated to zero thickness of lead, the integral number of protons above the bias, the ratio of neutrons to protons, and an estimate of the expected ratio of neutrons to protons. The estimate of the ratio of the neutron to proton counts is based on the assumption that the neutron and proton spectra are identical and is felt to be reliable to about a factor of two.(Appendix II). We must regard the rather close agreement with experiment as accidental.

Table III

Comparison of neutron and proton counts

E_B	N(cPb)	$P > E_B$	N/P	N/P calc.
Mev	counts/M2	counts/M2		(App.II)
20	$.55 \times 10^{3}$	10.5×10^{3}	.052	.047
40	.22	5.6	.039	.032
55	.076	3.8	.020	.022
70	.036	2.9	.012	.017
80	.017	2.4	.007	.013

B. Search for Neutron-Proton Coincidences

An experiment was performed designed primarily to detect possible neutron-proton coincidences. The data obtained to date are very meager but are consistent with what one would expect from the photoelectric disintegration of an n-p system in the nucleus.

C. Mesons

A by-product of the proton experiments was some preliminary data on π^--meson production in carbon. They are given in Table IV along with the Berkely results for π^+-mesons.(9)

Table IV

π^- Production at 90° by 300 Mev synchrotron photons on carbon

E_π	σ_{π^-}	σ_{π^+} (Ref. 9)
Mev	μb/Mev-ster-eff. quanta ± 50%	μb/Mev-ster-eff. quanta + 50% - 20%
55	.12 ± .05	.11 ± .01
57	.17 ± .05	.09 ± .01
60	.10 ± .02	.07 ± .007

The angle of observation was 90°.

It is only at this angle that the statistics are reasonably good. The rear counter was biased a few Mev above its thickness in energy for π -mesons. Under these circumstances we can reasonably expect that any π^- which stopped and produced a star (70% of the total stopping) (10) would have been counted with high efficiency. More precisely, if the π^- penetrated more than .2 of the way through the crystal, an additional energy of less than 15 Mev had to be lost by the star for a count to be recorded. π^+ mesons which $\pi^+ \rightarrow \mu^+ \rightarrow e^+$ decayed in the crystal within the rise time of the counter (about 10% of the total stopping) would have been counted if the decay electron had been emitted in an appropriate direction. This requirement reduced the probable efficiency for π^+ to a few per cent; hence the counter recorded essentially only π^-.

V Discussion of Results

A. Energy Spectrum

With the exception of a discrepancy of a factor 5 in the magnitude of the absolute cross-section (Table V below), the data of Fig. 7 join smoothly those of Silverman and Levinthal.(2) In the energy range from ~10 to 70 Mev they found a differential energy spectrum which was represented very well by an expression of the form:

$$d\sigma(E) \sim \frac{dE}{E^{\gamma}}$$

where δ increases with atomic number from 1.7 for carbon to 2.2 for lead. The solid curves in Fig.7 are an extrapolation of this spectrum normalized to give the best fit to the low energy points. The data fit nicely out to 150 Mev. Above this energy there is a break in the spectrum and the number of protons starts to decrease much more rapidly (approximately as the -8 power for carbon and the -7 power for cadmium if the correction for nuclear absorption is made). The slight increase in the exponents with increasing atomic number can be associated with scattering of the escaping protons by the nucleus and probably does not indicate a change in the production spectrum (Appendix III). Extrapolation to zero scattering would indicate a production spectrum falling off just slightly less rapidly than that observed for carbon.

It is of interest to compare the proton spectrum produced by 300 Mev bremsstrahlung with that obtained by Walker[1] for 198 Mev bremsstrahlung. Walker's observations show an integral spectrum falling off as the -4 power of the proton energy in the energy range 50-125 Mev. Unfortunately the statistics are not sufficiently good to enable one to deduce an accurate differential spectrum but the measurements would certainly be consistent with a differential spectrum similar to that observed at higher synchrotron energy with the break occuring at 80-90 Mev.

The occurance of a break in the energy spectrum at about half the maximum photon energy, W, suggests that the recoil part-

icle involved in the production of protons by photons is a single nucleon. If we imagined that the recoil were a three-nucleon system (as one might expect on a strict α-particle model), the break should occur at about $\frac{3}{4}W$, while the recoil of a two-nucleon system would put the break at $W/5$. The existence of a high energy tail above $\frac{1}{2}$ W leaves some ambiguity about the process. However, Levinger [5] has shown that for a two-nucleon model this tail may be completely explained by motion of two-nucleon systems in the nucleus and that one need not invoke any other processes.

B. Angular Distribution

The angular distributions (Figs. 8 and 9) show a strong forward asymmetry which increases with increasing proton energy. This behavior extrapolates smoothly from the data of Silverman and Levinthal. At 10 Mev they found an angular distribution which was isotropic, while at 40 Mev the distribution already showed a fairly strong forward asymmetry.

A comparison of the angular distribution obtained by Walker for 90 Mev protons with that found in the present experiment for 100 Mev protons shows good agreement for both the shape of the distribution and the magnitude of the cross-section. (See Table V below).

The forward asymetry on the angular distribution again rather favors a two-nucleon model since a photon could not in-

part sufficient forward momentum to a heavier system to produce such an asymmetry if the distribution in the CM system was primarily a dipole one. The argument is not too strong, however, because the distribution might well have an intrinsic forward asymmetry.

C. Z-dependence

Perhaps the one slightly surprising thing about the Z-dependence (Fig. 10) is that it should be so nearly proportional to the atomic number. At first thought one would expect a strict Z- or A-dependence to be modulated by a factor $A^{-1/3}$. However, an investigation of this point, which includes the effects of protons scattered into a given energy interval from a higher energy, shows that the modulation should be more nearly proportional to $A^{-1/6}$ (Appendix III). Assuming this modulation the data are fit nicely by a primary yield which varies as (A-Z)Z/A.

Silverman and Levinthal obtained virtually the same Z-dependence for 40 Mev protons as we obtained for 125 Mev protons.

D. Excitation Function

The excitation function for 105 Mev protons is shown in Fig. 11. To test the internal consistency of the data the expected yield curve was calculated assuming a spectrum similar to that observed at 300 Mev with the break occuring at $(E_c = B/2 - 15,$

where W is the maximum photon energy. An average binding of 15 Mev is assumed for the protons.

$$d\sigma(E) \sim \begin{cases} dE/E^{+1.7} & E < E_c \\ dE/E^{+6} & E > E_c \end{cases}$$

The curve in Fig. 11 represents the results of this calculation. It was normalized to Walker's point. It should be pointed out that a variation of ± 10 Mev in E_c or of ± 1 in the exponent of E for $E > E_c$ begins to destroy the fit rather badly. The fit is relatively insensitive to small changes in the exponent of E for $E < E_c$.

The excitation curve seems again to favor a single nucleon recoil although a threshold so near 150 Mev might also indicate a mesonic origin.

E. Absolute Cross-section

As has already been mentioned there is some discrepancy in the measurement of the absolute cross-section made by different experimenters. The values obtained for 70 Mev protons at 90° to the beam are compared in Table V.

Table V

	Method	Synchrotron Energy Mev	$\frac{d\sigma}{d\Omega}$ μb/Mev-ster-eff. quanta	Maximum likely error
Silverman & Levinthal	Proportional Counter	300	.15	factor 2
Walker	Photographic plates	300	.95*	55%
Keck	Scintillation counter	300	.74	50%

F. Neutrons

Preliminary experiments show that high energy neutrons are present in numbers consistent with approximate equality of the neutron and proton fluxes. This is to be expected since most processes which produce energetic protons will also produce energetic neutrons.

---

* The value given here is lower than that previously reported by Walker [1]. The change is associated with the improved measurements of the absolute beam intensity discussed in Section II, Part B of this paper.

VI Summary and Conclusions

Before proceeding to consider various interactions by which 200 and 300 Mev synchrotron radiation can produce energetic protons, we should like to summarize briefly the conclusions which can be drawn about the primary proton spectrum from the experimental observations. The primary spectrum will differ from the observed spectrum for two reasons: first, it will be shifted up in energy by the average binding energy for protons, and second, it will be modified by the scattering of the escaping protons by the residual nucleus. If we take these effects into account, a primary spectrum having the following characteristics is implied: (1) a yield proportional to NZ/A; (2) an energy distribution which falls off relatively slowly (as $E^{-1.7}$) up to half the maximum photon energy and then decreases rapidly (as E^{-6}); (3) an angular distribution in the laboratory system having a somewhat stronger forward asymmetry than that observed (Fig. 8).

The number of processes by which energetic photons can produce protons is quite large and increases as the energy of the protons decreases. Primarily for this reason, we shall confine our attention to the high energy end of the spectrum. We should like to emphasize the fact that all of the processes considered will produce <u>some</u> protons. It is the purpose of the discussion to indicate the angular and energy range in which each is most important. In treating the problem, we have, in general, avoided appealing to arguments involving measurements or calculations of absolute cross sections.

A. Isotropic Proton Production

We consider first those processes which are expected to produce energetic protons more or less isotropically in the laboratory system. They are (1) absorption of a photon to form a compound nucleus which subsequently emits a proton, (2) capture of a π^- meson at the end of its range to produce a star from which an energetic proton emerges, (11) and (3) creation and reabsorption of a meson in the same nucleus to produce a star from which energetic protons emerge.

Inspection of the observed angular distributions (Fig. 6, and Ref. 1, 2) shows that even though the fractional contribution from isotropic production may be large in the backward direction, it will always be small in the forward direction. This argument would certainly seem to rule out the possibility that any of the processes listed above could contribute the major fraction of the total cross-section.

Nevertheless, the process of meson creation and reabsorption is of sufficient interest to warrant slightly closer attention. First, the assumption of an isotropic distribution is based on the fact that the angular distribution of the mesons producing the protons is itself more or less isotropic (9), and one would certainly expect the proton distribution to be even more nearly isotropic. If this assumption were wrong the argument for small production in the forward direction breaks down. We could still argue that a process involving meson production should show a yield which rises quadratically with synchrotron energy above the meson threshold

(contrary to the observations of Fig. 11), but this argument is not so clear cut since we must also know how the reabsorption process depends on energy. Second, it has been proposed by Kikuchi (4) that meson absorption may be the explanation of the numerous photon stars observed in photographic plates. The cross-section for star production is comparable with that for the production of protons with energies over 50Mev. This could imply that meson interactions in the nucleus produce such protons which then make the stars. The strongest evidence that the stars are meson-produced is that there is a threshold for their production in the neighborhood of 150 Mev photon energy. In view of the apparent difficulty encountered in explaining the proton angular distribution on a meson absorption hypothesis, we feel it may be worthpointing out that there is an alternative explanation of this threshold based only on the assumption that a photon can produce one or two fast nucleons. Briefly, the argument [illegible] proceeds as follows: Since the production cross-section for protons is proportional to Z, we may expect that a large fraction of the stars will be produced in the heavy elements, Ag and Br, of the photographic emulsion. The stars produced in these elements will contain primarily evaporation prongs (12,10), and an analysis of the prong distribution indicates that there will be a relatively sharp threshold for the production of two or more prong stars somewhere in the range of photon energies from 100 to 150 Mev. The excitation function for star production can be expected to rise most rapidly a little above this threshold

and then to rise less and less rapidly as the maximum photon energy increases. This behavior may be contrasted with the quadratic rise with energy-above-threshold [12] that one might expect for meson-produced stars and may be a means for deciding between the two mechanisms.

B. Small Angle Proton Production

The next two processes which we shall consider can produce energetic protons only at small angles to the beam. They are (1) Compton scattering and (2) recoil from production of π^- and π° mesons. Some idea of the angular range in which these processes may be important can be obtained from an inspection of Table VI, in which we have tabulated the maximum angle of the recoil protons produced by 200 and 300 Mev photons on target nucleons having energies of 0 and 20 Mev.

Table VI

Synchrotron energy Mev	Energy of target nucleon Mev	Proton energy 75	100	125	150	175 Mev
		Max. Proton angle in degrees for Compton process				
300	0	34	16	-	-	-
300	20	76	64	48	35	17
200	0	-	-	-	-	-
200	20	57	34	-	-	-
		Max. Proton in degrees for meson production				
300	0	23	-	-	-	-
300	20	65	57	32	-	-
200	0	Max. proton energy = 45 Mev.				
200	20					

One sees immediately that both these processes will be much more important at 300 than 200 Mev synchrotron energy. Therefore, if their contribution to the proton cross-section were large, a comparison of the angular distributions for protons of a given energy produced by 200 and 300 Mev synchrotron radiation should show significantly more protons in the forward direction at the higher machine energy. This is contrary to the experimental results of Walker (1) and of the author which indicate identical distributions within the statistics. We conclude that even in the allowed angular range the contribution from Compton scattering and recoils from meson production is small.

C. Photo-electric Protons

A nuclear photo effect offers perhaps the most reasonable explanation of the large proton production in the forward direction. The process involves the absorption of a photon by the nucleus with the direct production of a fast nucleon and a recoil which may be the entire nucleus or any fraction thereof. The photo effect has been calculated on the basis of two different models for the nucleus and still others are possible. Those considered in some detail may be designated as the "one nucleon model" and the "deuteron model". A model not yet considered in detail is the "alpha particle model".

The "one nucleon model" has been investigated by Silverman and Levinthal. (2) They assumed an electric-dipole interaction with a proton having the momentum distribution of Chew and Gold-

berger [14] and, following the methods of Bethe and Peierls, [15] were able to calculate the variation of the total cross-section with energy of proton and photon. The proton is assumed to recoil against an infinitely heavy nucleus in this calculation. Their result is compared with the experimental data in Fig. 18. The fit is quite nice from 80 to 180 Mev. The excess production below 80 Mev can be easily understood as due to evaporation protons from nuclei heated by the more energetic protons and neutrons in their escape. The deficient production above 180 Mev could be explained as due to breakdown of the momentum distribution assumed for the nucleons. While a fit could thus be obtained for the 300 Mev data, the theory could not simultaneously fit the observed excitation function or Walker's data at 200 Mev. An alternative explanation of the break at half the maximum photon energy is that it is not the entire nucleus that takes up the recoil but a small number of nucleons which carry off about half the photon energy.

We should point out that in Fig. 18 we have compared a calculated total cross-section with an observed differential cross-section. This is permissible since we are only interested in the shape of the curve and the differential cross-section at 87.5° is nearly proportional to the total cross-section.

As we have previously mentioned, the experimental results suggest that the recoil involved in the proton production is a single nucleon. A model of this type explains qualitatively the break in the energy spectrum and the forward asymmetry in the ang-

ular distribution. J.S. Levinger[6] has investigated theoretically such a model. Levinger's analysis is based on the reasonable assumption that the very high momentum components of the nuclear wave function are similar to those of the deuteron wave function. The theory predicts a cross-section of .29 μb/Mev-ster-eff. quanta for the production of 70 Mev protons at 90° to the beam by 300 Mev synchrotron radiation. The uncertainty in the theoretical cross-section is a factor of 3. A comparison with the experimental values in Table V shows satisfactory agreement. The energy spectrum is compared with the experimental data in Fig. 15. Unfortunately the conditions for the validity of the model are not well satisfied for the energies important in the experiments so the fact that the curve does not fit the observed distribution in the important range up to 150 Mev is not surprising. Above 150 Mev the curve fits the data nicely. This can be attributed to the fact that the energy spectrum above this point is determined primarily by the momentum distribution of pseudo-deutrons in the nucleus and is relatively insensitive to the details of the production process below the "cut off". The agreement obtained above the "cut off" lends some support to the assumption of an interaction with a two-nucleon system. The angular distribution predicted by the theory is compared with the experiment in Fig. 8. Magnetic interactions and the effects of scattering in the nucleus were neglected. In view of this, the fit with the experimental points seems reasonable. The model, of course, also fits the Z-dependence and the excitation function.

Unfortunately there are no detailed calculations of the photo-effect based on the alpha-particle model of the nucleus. This model should certainly give a better approximation to the nuclear wave function than the deuteron model and therefore holds promise. The principal objections to an α-particle model are that the recoil of a triton is not favored by the position of the break in the energy spectrum (Fig. 13) and it is not easy to develop a strong forward asymmetry in the angular distribution.(Fig 6)

The conclusion which it seems one can draw from the foregoing discussion is that at the present time there is no model for which calculations have been made which predicts in detail all the features of the large proton production in the forward direction. Nevertheless, the partial successes of both the one nucleon and the deuteron models hold out the hope that a model which assumed an electo-magnetic interaction of a photon with a neutron-proton pair having the correct momentum distribution (obtained either empirically or theoretically) would come fairly close to the mark.

Appendix I

A. Range Energy Relations

The design and calibration of the counter telescope as well as the analysis of the data rests upon the assumption of a range-energy relation for the particles being studied. In this appendix we give a brief summary of the points involved.

The range-energy relation for protons was obtained from a semi-empiracal nomograph prepared by R.R.Wilson. In the energy range from 2 to 800 Mev. it may be represented by the following expression:

$$\frac{R}{R_0} = \left(\frac{E}{E_0}\right)^{\beta} \qquad (1)$$

Values of R_0 corresponding to E_0 = 100 Mev and β are tabulated for a few elements in Table VII, Part A.

Table VII

Part A E_0 = 100 Mev

Element	β	R g/cm²	R_0(Al) / R_0	$\frac{dE}{dR} \Big/ \frac{dE}{dR}$ (Al)
H	~ 1.78	~ 8.3	~ 2.65	~ 2.62 (16)
Be	~ 1.76	9.4	1.02	1.02 (16)
C	1.76	8.5	1.13	1.13
Na	1.76	9.4	1.03	1.03
Al	1.76	9.6	1.00	1.00
Cu	1.75	11.6	.83	.835
Cd	1.74	13.5	.71	.72
I	1.73	14.0	.69	.70
Pb	1.72	16.0	.60	.61

Part B

Compound		
NaI	12.9	.75
Xylene $C_8 H_{10}$	7.5	1.28
Anthracene $C_{14} H_{10}$	7.8	1.23

The variation in β for different elements is slight. In the range of validity of equation (1), it is a good approximation to set β equal to 1.75 for all elements. This assumption makes the relative stopping power of different elements independent of energy so that the stopping power of a compound or inhomogeneous medium may be unambiguously calculated from the stopping power of its components without regard to distribution. The values of R_o for NaI and xylene listed in Table VI, Part B, were calculated with this assumption in mind.

The range-energy relation for a particle of arbitrary mass and charge may be calculated from that for a proton with the help of the well-known formula

$$(2) \qquad R_{M_2 Z_2}(E) = \frac{M_2}{M_1} \left(\frac{Z_1}{Z_2}\right)^2 R_{M_1 Z_1}\left(\frac{M_1}{M_2} E\right)$$

B. Interpretation of Proportional Counter Data

Consider the case of a proportional counter on which protons of all energies are incident. The largest pulses produced in the counter will be due to those protons with a range just equal to the thickness of the counter. A given pulse height less than maximum (but greater than that due to a minimum ionization proton) will correspond to protons of two different ranges, one greater and the other less than the thickness of the counter. It follows that if one sets a bias on the counter such that only pulses greater than a given height are counted, one has effectively defined a range interval in which a particle must stop in order

to be counted.

In Fig.14, we have plotted several relations which have been found useful in the quantitative interpretation of the results obtained from proportional counters. It is convenient to chose the thickness of the counter, R_o, as the unit of range and the corresponding energy, E_o, as the unit of energy. All relations given have been derived from the range-energy relation:

$$r = \epsilon^{1.75} \tag{3}$$

where $r = \frac{R}{R_o}$ and $\epsilon = \frac{E}{E_o}$. This relation is shown by Curve 1.

The first derived quantity of interest is the energy lost in a counter by a particle having a residual range ($r^* - 1$). This is simply:

$$\epsilon_1 \equiv \epsilon(r^*) - \epsilon(r^* - 1)$$

$$= r^{*1/\beta} - (r^* - 1)^{1/\beta} \tag{4}$$

We may regard equation 4 as defining the quantity r^*. This relation is plotted as Curve 2. For $r^* >> 1$, we may expand (4) to obtain the approximate expression

$$\epsilon = \frac{1}{\beta} r^{*-(1-1/\beta)} \left[1 + \frac{1}{2}\left(1 - \frac{1}{\beta}\right) r^{*-1} + \cdots \right] \tag{5}$$

The leading term in the expansion is just the specific ionisation of a particle of residual range r^*.

The second derived quantity of interest is the range interval, Δr , in which a particle must stop to lose an energy greater than ϵ_1 in a counter.

$$\Delta r \equiv r^*(\epsilon_1) - r(\epsilon_1) \tag{6}$$

This relation is plotted as Curve 3. For $\epsilon \sim 1$, Δr is a linear function of $1-\epsilon_1$. This is shown by Curve 4.

The last derived quantity of interest is the mean range, $\bar{r}$, of a particle stopping at random in Δr.

$$\bar{r} \equiv r(\epsilon_1) + \frac{1}{2}\Delta r \tag{7}$$

This relation is shown by Curve 5.

The curves in Fig. 2, together with the data in Table II and equation 1, completly define a proton passing through a proportional counter in terms of the energy lost to the counter.

Appendix II

Neutron Counter Efficiency

The neutron counter used in these experiments consisted of a cylinder approximately 2" in diameter by 3" long containing a liquid hydrocarbon; the counter was shielded by 2" of lead. The following calculation was made in an attempt to estimate the counting efficiency of such an arrangement. It is divided into three parts. In Part A we estimate the efficiency due to hydrogen recoils; in Part B we estimate the efficiency due to neutron-induced stars in the carbon; in Part C we calculate the average efficiency for a $E^{-\gamma} dE$ spectrum.

Part A

Counting Efficiency due to Hydrogen Recoils

Let $Q(E,E')$ be the probability that a neutron of Energy E produces a recoil proton of energy E', and $P(E',E_B)$ be the probability that a proton of energy E' loses an energy greater than E_B to the counter. The efficiency is then:

$$\epsilon_H(E,E_B) = \int_{E_B}^{E} Q\,P\,dE' \qquad (1)$$

In order to calculate ϵ_H we assume first that the recoil protons are uniformly distributed in energy up to the neutron energy and second that all recoils are in the forward direction. With these two assumptions we may write for Q:

$$Q = \sigma_{np} N_H \frac{1}{E} \qquad (2)$$

and for P:

$$(3) \qquad P = 1 - \frac{R(E') - R(E' - E_B)}{L}$$

where R(E) denotes the range of a particle of energy E and L is the length of the counter. The RHS of (3) is just the ratio of the volume for which recoils are counted to the total volume. We use the following simple approximation for P(E), which is a slight overestimate:

$$(4) \qquad P \approx \begin{cases} 0 & : E' < E_B \\ 1 - \frac{R(E_B)}{L}\,\frac{E'}{E_B} & : E_B < E' < E_B\,\frac{R(E_B)}{L} \\ 0 & : E_B\,\frac{R(E_B)}{L} < E' \end{cases}$$

Inserting (2) and (4) in (1) and integrating, we obtain

$$(5) \qquad \epsilon_H \lesssim \begin{cases} \frac{\sigma_{np} N_H E_B}{2E}\left(\frac{E}{E_B} + \frac{E_B}{E} - 2\right) & : E < E_B\,\frac{R(E_B)}{L} \\ \frac{\sigma_{np} N_H E_B}{2E}\left(\frac{L}{R(E_B)} + \frac{R(E_B)}{L} - 2\right) & : E > E_B\,\frac{R(E_B)}{L} \end{cases}$$

The error in ϵ_H is primarily due to the approximation of forward scattering involved in the writing of equation (3). For $R(E_B) \ll L$, (3) should be very nearly correct. For $R \sim L$ our assumption overestimates the number of protons lost through the back of the counter and underestimates the number lost through the sides. While these two effects tend to cancel, the latter will certainly dominate and hence ϵ_H will be an overestimate.

Part B

Counting Efficiency due to Carbon Stars

In order to calculate the counting efficiency due to carbon stars, we need to know not only the cross-section for star pro-

duction as a function of neutron energy and star size but also something about the way in which the energy is distributed among the prongs. Since this detailed information is not available, we must make the best approximation we can.

We assume that the cross-section for star production is equal to the absorption cross-section of carbon for neutrons; it cannot be larger than this and measurements of Hadley and York[17] on protons and deuterons produced by 90 Mev neutrons on carbon indicate that it is not much smaller. It is also assumed that the stars are distributed uniformly in energy up to the neutron energy. There is some evidence that this is nearly the case for stars in heavy elements[18]. The last assumption we make is that all the ionizing prongs stop in the counter. This may be rather bad, especially in the case of very high energy stars in which most of the energy is probably carried away by a single high energy proton or deuteron. With these assumptions we may write:

$$\epsilon_c \lesssim \sigma_c^a N_c \left(1 - \frac{E_B}{E}\right)$$

For the energy range of interest, 20 to 150 Mev, σ_c^a is relatively insensitive to energy and we shall assume an average value $\sigma_c^a \approx .6\,\sigma_{geom.}$ for computational purposes.[19]

Part C

Integration over a Spectrum

If the neutrons incident on our counter are characterized by a differential energy spectrum $E^{-\gamma} dE$, the average efficiency as a function of E_B may be written:

$$\bar{\epsilon} \approx \int_{E_B} (\epsilon_H + \epsilon_c) E^{-\gamma} dE \Big/ \int_{E_B} E^{-\gamma} dE \qquad (6)$$

The integration of (6) is trivial. The formulae are rather lengthy, however, and will not be set down. Some numerical results for $\gamma = 1.7$ are given in Table VIII below.

Table VIII

Efficiency of Neutron Counter

E_B	$\bar{\epsilon}_H$	$\bar{\epsilon}_c$	$\bar{\epsilon}_H + \bar{\epsilon}_c$
20	.024	.023	.047
40	.012	.020	.032
55	.005	.017	.022
70	.002	.015	.017
80	-	.013	.013

In the above calculation we have neglected the contribution to the counting efficiency of processes in which ionizing secondaries produced in the lead surrounding the counter enter the active volume and are recorded. These processes may contribute an additional 10 to 20 % to the overall efficiency; a much larger contribution seems unlikely, except possibly at high bias where a proton must spend nearly the maximum possible energy on the counter to be recorded.

We wish to emphasize that the calculations given here are quite crude and are intended only to give a rough estimate of the neutron counting efficiency.

Appendix III

Escape of Protons from a Nucleus

In this appendix we give the details of a calculation made in an attempt to estimate the extent to which the "primary" proton spectrum is modified by interaction of the escaping protons with the residual nucleus. Following the suggestion of Serber, we consider the collisions of the escaping proton with the individual nucleons. The calculations parallel those of Goldberger and Fernbach, Serber, and Taylor [13] on the passage of high energy neutrons through nuclear matter.

The work is divided into three parts. In Part A we give an expression for the absorption coefficient of nuclear matter for protons as a function of energy. In Part B we give expressions for the probability of a definite number of collisions for one and two escaping nucleons. In Part C we apply the results of the preceding parts to the problem of the escaping protons.

Part A

Absorption Coefficient of Nuclear Matter for Protons

According to Fernbach, Serber, and Taylor the absorption coefficient for nuclear matter is equal to the particle density times the cross-section for individual nucleon-nucleon collisions.

$$K_i = \frac{3A}{4\pi R^3}\,\sigma_i \tag{1}$$

where

$$\sigma_i = \frac{Z}{A}\,\sigma_{ip} + \frac{A-Z}{A}\,\sigma_{in} \tag{2}$$

The subscript i is used to designate the incident nucleon, a proton or neutron. The cross-sections indicated in (2) are those for a free nucleon on a bound nucleon and will differ from the free-free cross-sections in that a certain fraction of the collisions inside a nucleus will be forbidden by the exclusion principle. A detailed analysis of this effect has been made by Goldberger.[18] He finds that for isotropic scattering, the free-free cross-sections are reduced by the fraction

$$(3) \qquad \frac{\sigma_{iP}}{\sigma_{iP}^{f}} = \left(1 - \frac{7}{5}\frac{E_f}{E}\right) \qquad : E > 2E_f$$

where E is the energy of the incident nucleon inside the nucleus and E_f is the Fermi energy. The expression is valid for E greater than twice E_f. The available data on the p-p interaction at high energies indicate nearly isotropic scattering and we shall assume eq. (3) to apply with $E_f = 22$. For n-p scattering which is not isotropic at high energy, eq. (3) is an underestimate. Goldberger has used the observed n-p scattering to calculate a better value for neutron energies of 66 and 117 Mev. The ratios of σ_{iP} to σ_{iP}^{f} at these energies are respectively .89 and .32. If we assume the form of eq. (3) to be correct and regard E_f as an adjustable parameter, a reasonable fit to the calculated points is obtained for $7/5\ E_f = 40$ Mev. Combining eqs. (1), (2), and (3) and assuming a 1/E dependence for the cross-sections*, we arrive

---

* The assumption of a 1/E dependence for p-p cross-section is correct only up to energies a little over 100 Mev. Failure of the 1/E law above 100 Mev. will not seriously affect our results in the range of energies up to about 150 Mev. where we wish to apply them.

at the absorption coefficient as a function of energy:

$$K_p = \frac{3A}{4\pi R^3}\left\{\frac{Z}{A}\frac{\sigma_{pp}^f}{E}\left(1-\frac{30}{E}\right)+\frac{A-Z}{A}\frac{\sigma_{np}^f}{E}\left(1-\frac{40}{E}\right)\right\}$$

a.

(4)

$$b.\ K_n = \frac{3A}{4\pi R^3}\left\{\frac{Z}{A}\frac{\sigma_{np}^f}{E}\left(1-\frac{40}{E}\right)+\frac{A-Z}{A}\frac{\sigma_{nn}^f}{E}\left(1-\frac{30}{E}\right)\right\}$$

The n-p and p-p scattering cross-sections have been measured (20, 21, 22). We take the n-n cross-section equal to the p-p cross-section. A fair approximation is $2\sigma_{nn}^f = 2\sigma_{pp}^f = \sigma_{np}^f = .075$ barns at 100 Mev incident nucleon energy. In setting $2\sigma_{nn}^f \approx \sigma_{np}^f$ we differ slightly from Goldberger who assumed $4\sigma_{nn}^f = \sigma_{np}^f$. Inserting the values for the cross-sections and setting $\frac{Z}{A} = \frac{1}{2}$, we find the following expression for K which is valid for protons or neutrons:

$$K = 5.2 \times 10^{14}\frac{1}{E}\left(1-\frac{35}{E}\right) \qquad : E > 44\ \text{Mev} \tag{5}$$

where E is in Mev. In evaluating (4) to obtain (5) we have used the expression $R = 1.37\ A^{1/3} \times 10^{-13}$ cm. Equation (5) gives a value of K about 40% greater than that used by Fernbach et al. to fit the 90 Mev neutron cross-sections. However, their calculations are relatively insensitive to K and the value given by (5) would fit the data as well.

Part B.

Collision Probabilities for a Spherical Nucleus

In this section we calculate the probability that a nucleon traversing a nucleus with an energy of the order of 100 Mev makes

a definite number of collisions. We adopt a classical approach in which the concepts of a definite trajectory for the nucleon and a well-defined radius for the nucleus are used. We assume that the paths of the particles are undeviated in a collision and that the initial value of K, the "collision coefficient", applies over the whole trajectory. These approximations are fairly well justified for a wide range of practical applications bythe relative insensitivity of the results to Ra.

The calculation is made for three closely related cases:

CaseI. Consider the case of a homogeneous beam of nucleons incident on a spherical nucleus having a "collision" coefficient K. Let $P_o(n)$ be the probability that an individual nucleon makes exactly n collisions in traversing the nucleus.

$$P_o(n) = \frac{1}{\pi R^2} \int_0^R 2\pi r\, dr \frac{(2Ks)^n}{n!} e^{-2Ks}$$

where $s^2 = R^2 - r^2$

Integration yields:

$$(7) \quad P_o(n) = \frac{2(n+1)}{(2KR)^2} \left\{ 1 - e^{-2KR} \sum_{l=0}^{n+1} \frac{(2KR)^l}{l!} \right\}$$

$P_o(n)$ is tabulated in Part A of Table IX for n=0, 1, 2.

Case II. Consider the case in which a pair of nucleons moving in opposite directions are formed with uniform probability throughout the interior of a spherical nucleus. Let $P_2(n,m)$ be the probability that one partner makes exactly n collisions while the other partner makes exactly m.

$$P_2(n,m) = \frac{3}{4\pi R^3}\int_0^R 2\pi r\,dr \int_0^{25} \frac{(Kx)^n}{n!} e^{-Kx} \frac{(2Ks-Kx)^m}{m!} e^{-2Ks+Kx}\,dx$$

where $s^2 = R^2 - r^2$.

Integration yields:

$$P_2(n,m) = \frac{3(n+m+2)}{(2KR)^3}\left\{1 - e^{-2KR}\sum_{l=0}^{n+m+2}\frac{(2KR)^l}{l!}\right\} \tag{8}$$

$$= \frac{3}{2}\frac{1}{(2KR)}\,P_0(n+m+1)$$

Note that $P_2(n,m)$ is a function of the total number of collisions $n+m$. $P_2(n,m)$ is tabulated in Part B of Table IX for $n+m = 0,1,2$.

CaseIII. Consider the case of a single nucleon produced at random in the interior of a spherical nucleus. Let $P_1(n)$ be the probability that it makes exactly n collisions in escaping. $P_1(n)$ may be obtained either by direct calculation or by summing $P_2(n,m)$ over all collisions of one partner.

$$P_1(n) = \sum_{m=0}^{\infty} P_2(n,m)$$

$$= \frac{3}{2}\frac{1}{2KR}\left\{1 - \sum_{k=0}^{n}\frac{2(k+1)}{(2KR)^2}\left(1 - e^{-2KR}\sum_{l=0}^{k+1}\frac{(2KR)^l}{l!}\right)\right\} \tag{9}$$

$$= \frac{3}{2}\frac{1}{2KR}\left\{1 - \sum_{k=0}^{n} P_0(k)\right\}$$

$P_1(n)$ is tabulated in Part C of Table IX for $n = 0, 1, 2$.

Table IX

Collision Probabilities for Spherical Nucleus

RK	.25	.5	.75	1.0	1.5	2	3
Part A: $P_0(n)$							
n							
0	.722	.528	.392	.297	.178	.114	.055
1	.232	.321	.339	.322	.256	.190	.104
2	.044	.113	.175	.214	.235	.212	.142
Part B: $P_2(n,m)$							
n↓m							
0	.696	.482	.339	.242	.128	.071	.026
1	.131	.169	.175	.161	.118	.080	.036
2	.017	.040	.067	.080	.082	.069	.040
Part C: $P_1(n)$							
P							
0	.835	.709	.608	.527	.411	.332	.236
1	.138	.226	.269	.296	.283	.261	.210
2	.007	.057	.094	.125	.166	.181	.175

Part C.

Escape of Protons from a Nucleus

Let $N_0(E)\,dE$ be the differential energy spectrum of protons produced in a primary process in the interior of a nucleus. If E is the energy of the particle inside the nucleus and V is the depth of the potential well, then the number of protons escaping with energy E-V will be equal to the number, $P_1(0)N_0(E)$, escaping without suffering a collision plus the number, $SN_0(E)$, scattered into the energy interval (E, E + dE) from a higher energy.

$$N(E-V) = \left(P_1(0) + S\right) N_0(E) \tag{10}$$

$P_1(0)$ may be obtained directly from the results of the two preceding Parts. S(E) may be estimated as follows: If we assume that the scattered protons are distributed uniformly in energy from approximately 20 to (E' - 10) Mev., where E' is the energy of the incident proton, and restrict our attention to those processes in which a proton escapes with more than half the energy of the primary proton, we may write:

$$S = a\,P_1(1)\,N_0^{-1}(E) \int_{E+10}^{2E} N_0(x)\, d\ln(x-30) \tag{11}$$

$$+ b\,P_1(2)\,N^{-1}(E) \int_{E+20}^{2E} \int_{E+10}^{x-10} N_0(x)\, d\ln(x-30)\, d\ln(y-30)$$

$$+ \cdots$$

In writing (11) we have neglected the slight energy dependence of $P_1(1)$ and $P_1(2)$. The coefficients a and b are numbers which involve essentially the relative probability of various sequences of collisions. Since it is almost certain that neutrons with a spectrum similar to the proton spectrum are also produced, a and b should include terms describing processes in which a neutron may give rise to an escaping proton. Expressions for a and b follow:

$$a \approx \frac{\sigma_{np} + 2\sigma_{pp}}{\sigma} + \frac{\sigma_{np}}{\sigma} = 2$$

$$b \approx \frac{(\sigma_{np} + 2\sigma_{pp})^2 + \sigma_{np}^2}{\sigma^2} + \frac{2\sigma_{np}(\sigma_{np} + \sigma_{pp} + \sigma_{nn})}{\sigma^2} = 4$$

The integrals appearing in (2) have been evaluted graphically inserting for $N_0(E)$ the observed spectrum for carbon $N(E-V)$. In the energy range from 50 to 130 Mev. for which the theory given should be a reasonable approximation, the results may be expressed by the following relation:

$$P_1(o) + S \sim A^{-1/6} E^{-\eta(A)} \qquad (12)$$

where $\eta(A)$ equals 0 for Carbon, .1 for copper, and .2 for lead.

Our investigation was originally undertaken to see how the dependence of the primary process on Z was modulated by A. An additional fact which emerges is that we should also expect a modification of the differential energy spectrum, which depends on A. It should be pointed out that the inclusion of higher order terms in S and low energy protons which were neglected will slight-

ly decrease in magnitude the exponent of A and will give a somewhat stronger dependence of η, the exponent of δ, on A.

Bibliography

(1) Walker, D., Phys. Rev. 81, 634 (1951)

(2) Silverman, A. and Levinthal, S., Private communication. Report submitted for publication in Phys. Rev.

(3) Kikuchi, S., Phys. Rev. 80 492 (1950)

(4) Kikuchi, S., PR 81, 1060 (1951)

(5) Levinger, J. S., Private communication. Report submitted for publication in Phys. Rev.

(6) Desire, J., Measurements made with Cornell pair spectrometer

(7) Wilson, R. R., Private communication. Cornell range-energy nomograph. See also (15).

(8) Reynolds, G. T., Harrison, F. B., and Salvini, G., Phys. Rev. 78, 488 (1950).

(9) Steinberger, J., and Bishop, J. S., Phys. Rev. 78, 494 (1950)

(10) Menon, M.G.K., Muirhead, H., and Rochat, O. Phil. Mag. Ser. 7, XLI, 583 (1950).

(11) See, e. g., Chesten, W. B., and GoldEarb, L.J.B. Phys. Rev. 78, 685 (1950).

(12) Perkins, D. H., Phil Mag. Ser 7, XL, 681 (1949).

(13) Bishop, A. S., Steinberger, J., and Cook, L. J., Phys. Rev. 80, 291 (1950).

(14) Chew, G. F., and Goldberger, M. L., Phys. Rev. 77, 470 (1950)

(15) Bethe and Peierls, Proc. Roy. Soc. A148, 146 (1935)

(16) Bakker, C. J., and Segre,,E., Phys. Rev. 81, 489 (1951).

(17) Hadley, J., and York, H., Phys. Rev. 80, 345 (1950).

(18) Goldberger, M. L., Phys. Rev. 74, 1269 (1948).

(19) Fernbach, S., Serber, R., and Taylor, T. B., Phys. Rev., 75, 1352 (1949).

(20) Birge, R.W., Phys. Rev. 80, 490 (1949).

(21) Panofsky, W.K.H., and Fillmore, F. L., Phys. Rev. 79, 57 (1950).

(22) Cook, L. H., McMillan, E. M., Peterson, J. M., and Sewell, D. C., Phys. Rev. 75, 7 (1949).

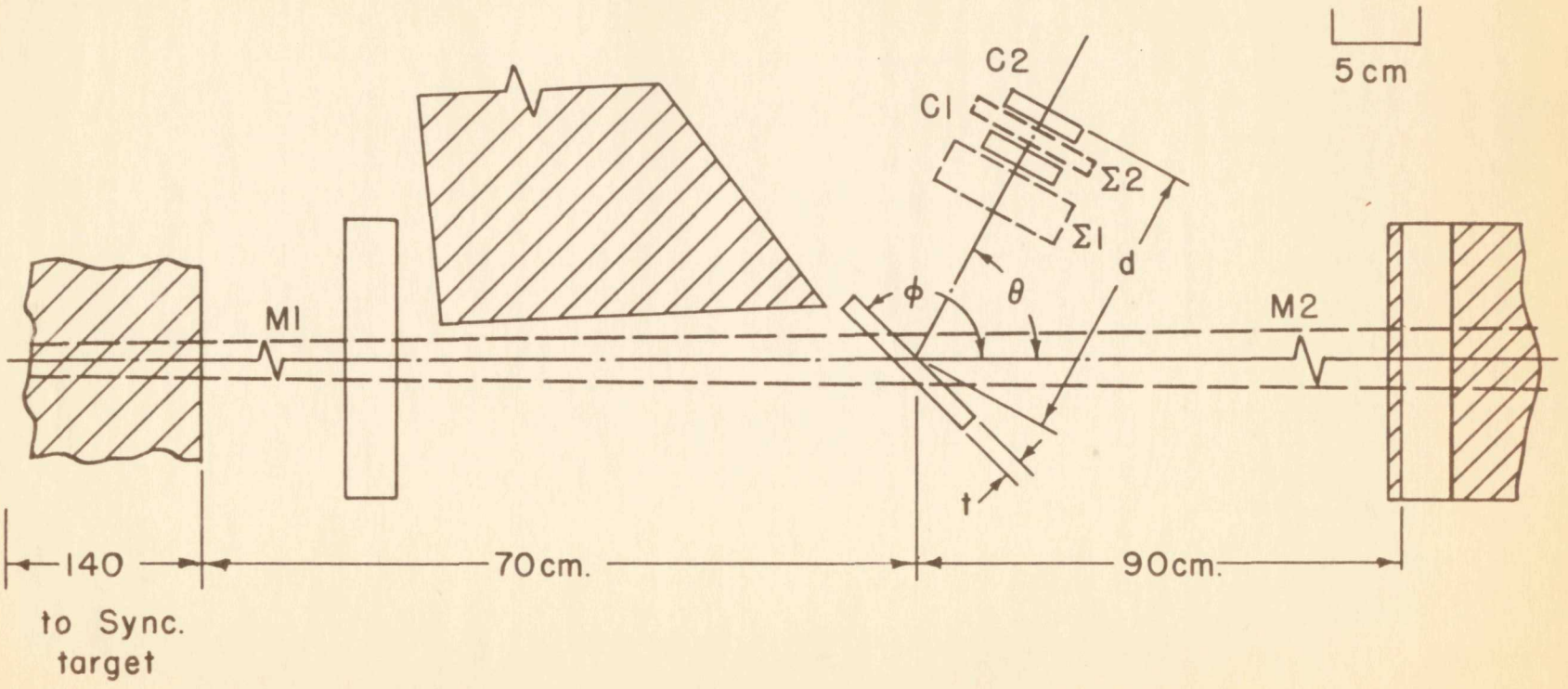

Fig. 1

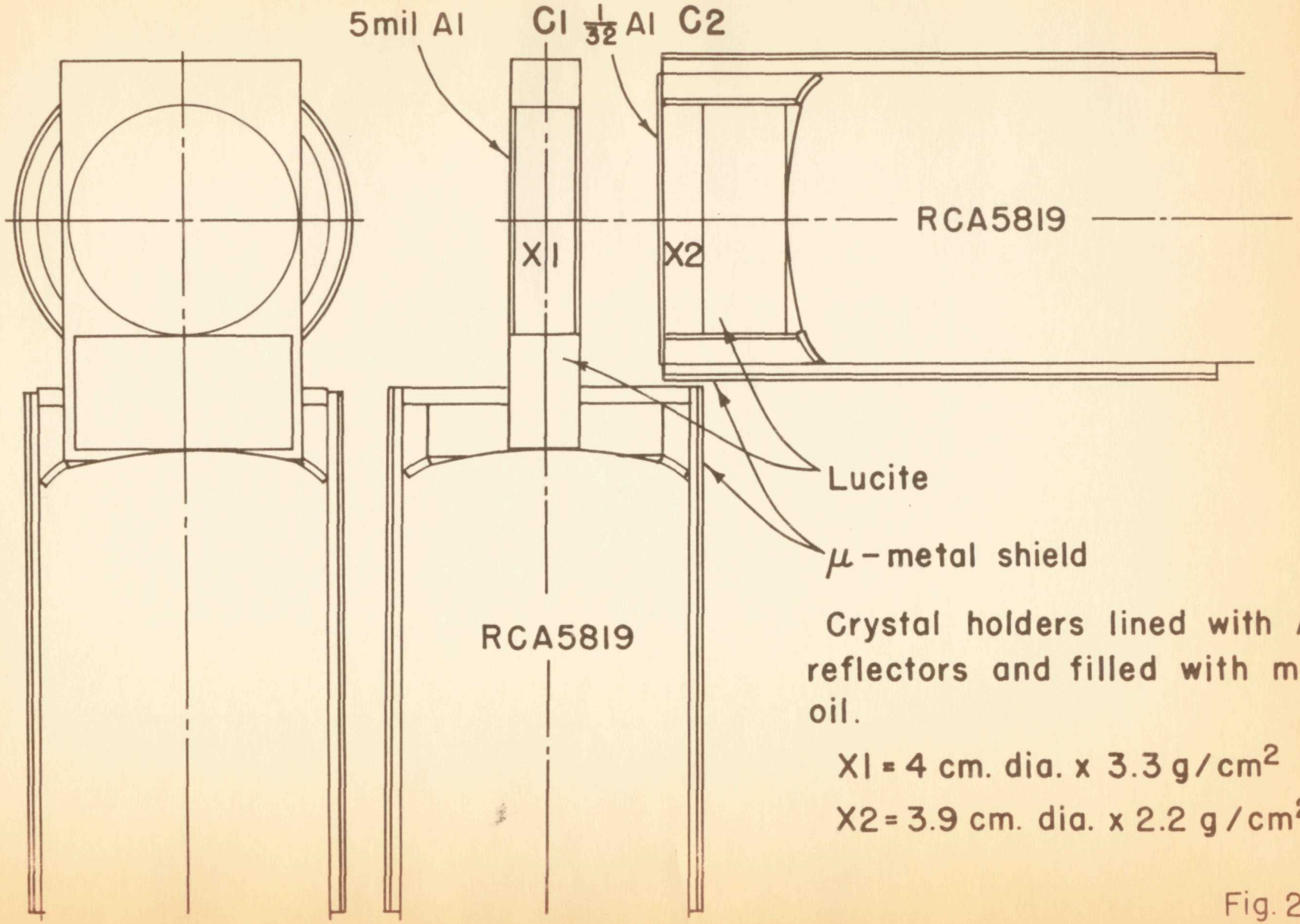

Crystal holders lined with Al reflectors and filled with mineral oil.

X1 = 4 cm. dia. x 3.3 g/cm^2

X2 = 3.9 cm. dia. x 2.2 g/cm^2

Fig. 2

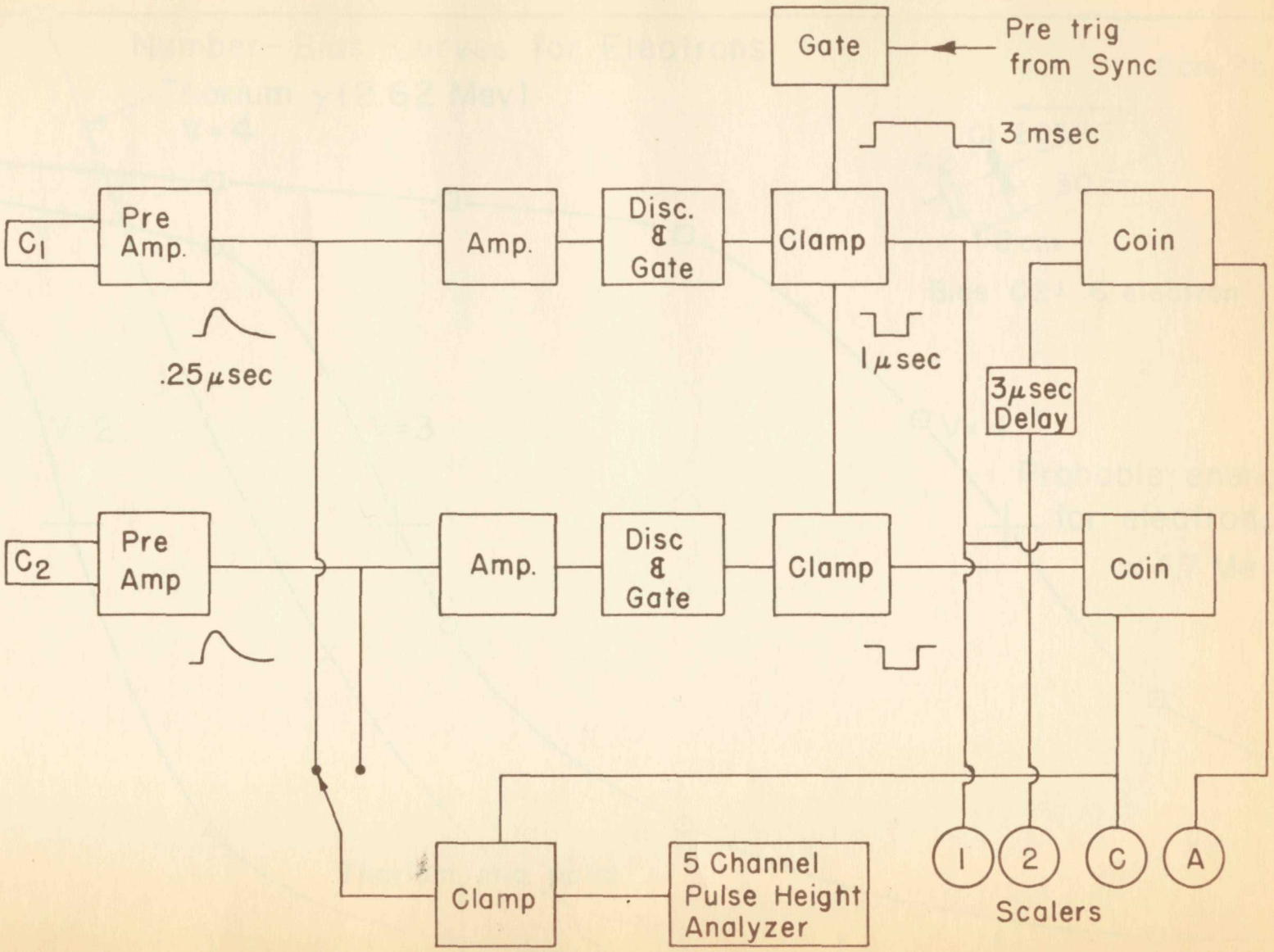
Gate
Pre trig from Sync
3 msec
C1
Pre Amp.
Amp.
Disc. & Gate
Clamp
Coin
.25 μsec
1 μsec
3 μsec Delay
C2
Pre Amp
Amp.
Disc & Gate
Clamp
Coin
Clamp
5 Channel Pulse Height Analyzer
1
2
C
A
Scalers

Fig. 3

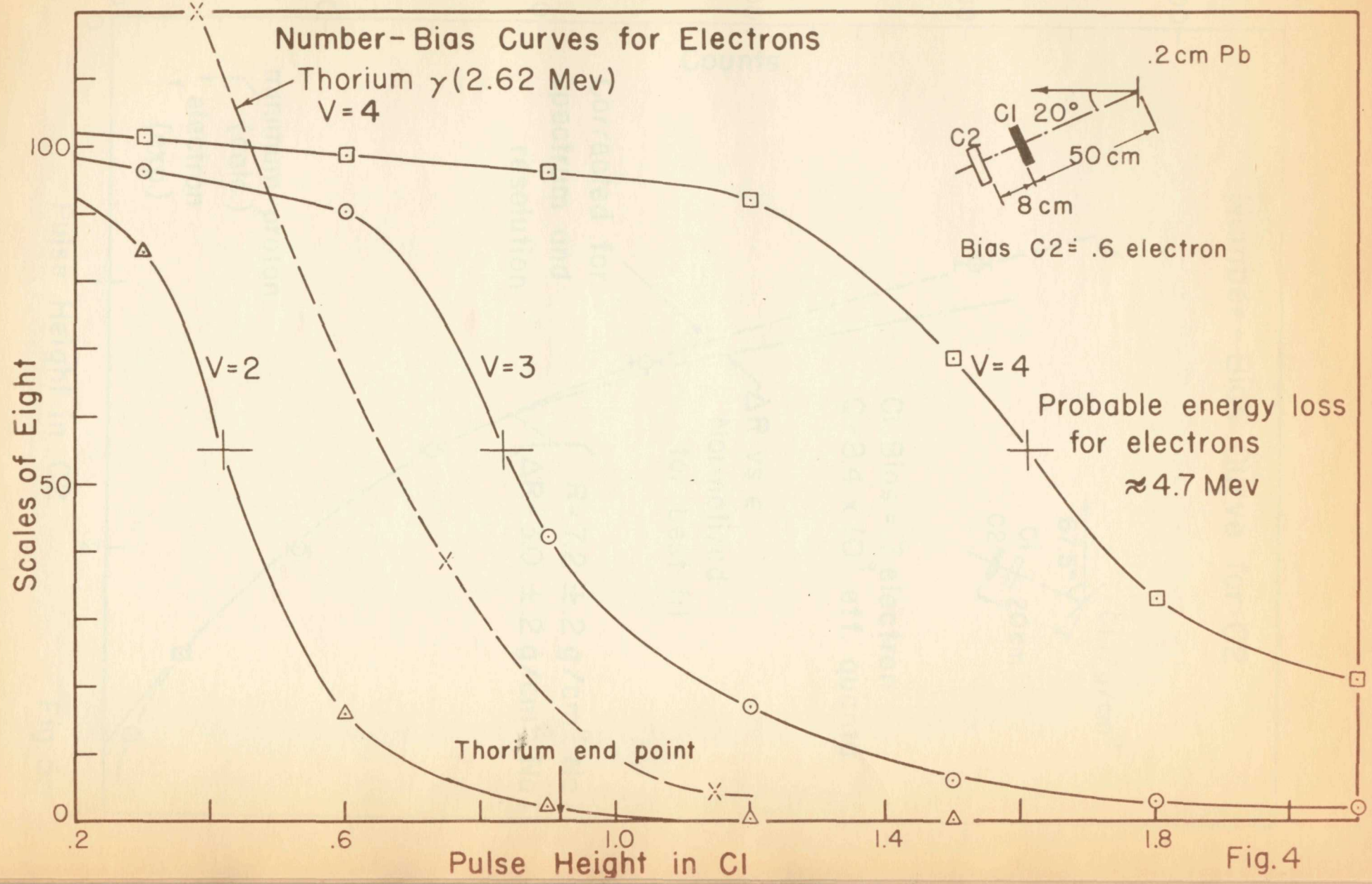
Number-Bias Curves for Electrons
Thorium γ (2.62 Mev)
V=4
.2 cm Pb
C1
20°
C2
50 cm
8 cm
Bias C2 ≐ .6 electron
V=2
V=3
V=4
Probable energy loss
for electrons
≈4.7 Mev
Thorium end point
Scales of Eight
100
50
0
.2
.6
1.0
1.4
1.8
Pulse Height in C1

Fig. 4

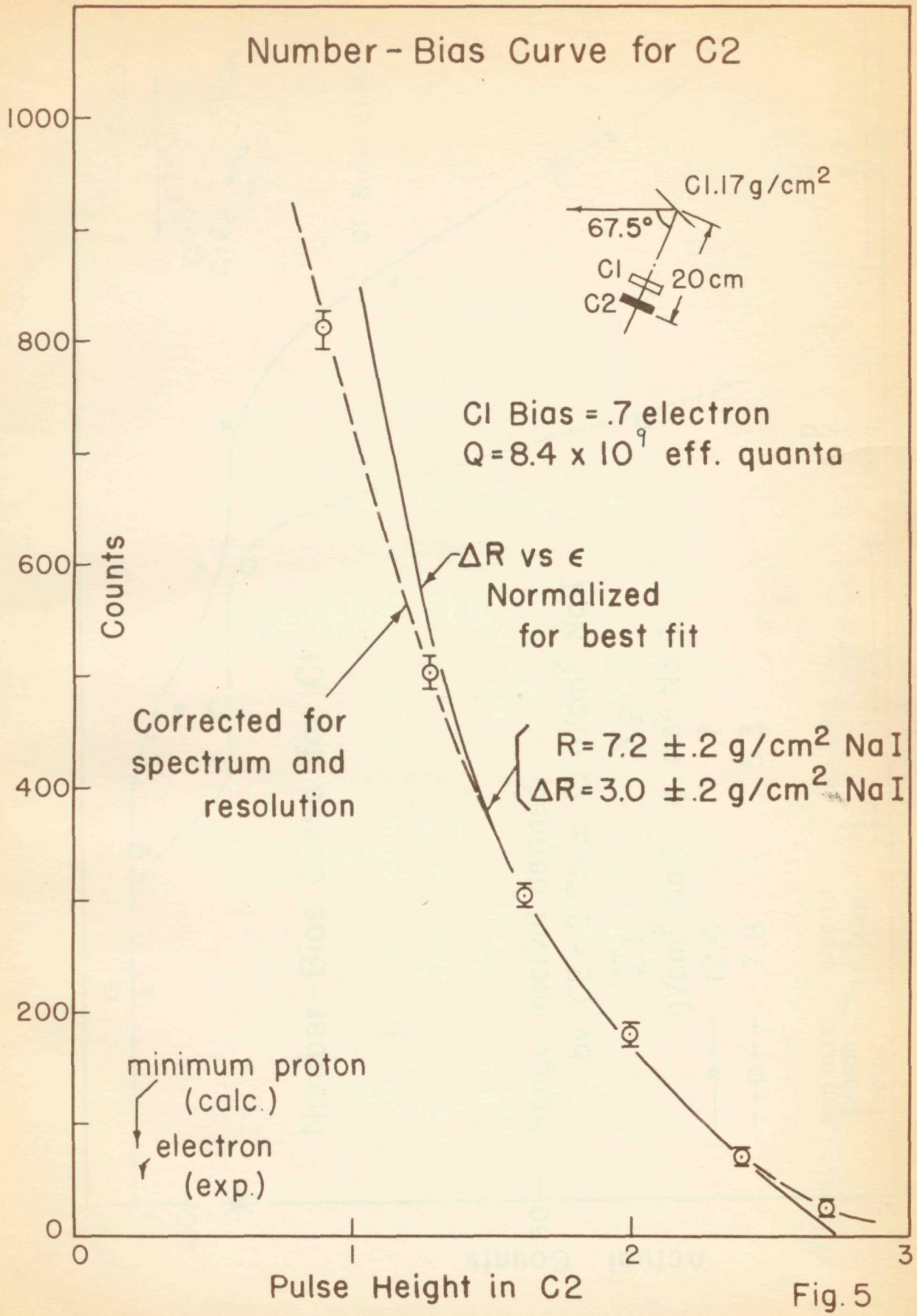
Number - Bias Curve for C2
1000
800
600
400
200
0
Counts
C1.17 g/cm²
67.5°
C1
20 cm
C2
C1 Bias = .7 electron
Q = 8.4 x 10⁹ eff. quanta
ΔR vs ϵ
Normalized
for best fit
Corrected for
spectrum and
resolution
R = 7.2 ±.2 g/cm² NaI
ΔR = 3.0 ±.2 g/cm² NaI
minimum proton
(calc.)
electron
(exp.)
0
1
2
3
Pulse Height in C2

Fig. 5

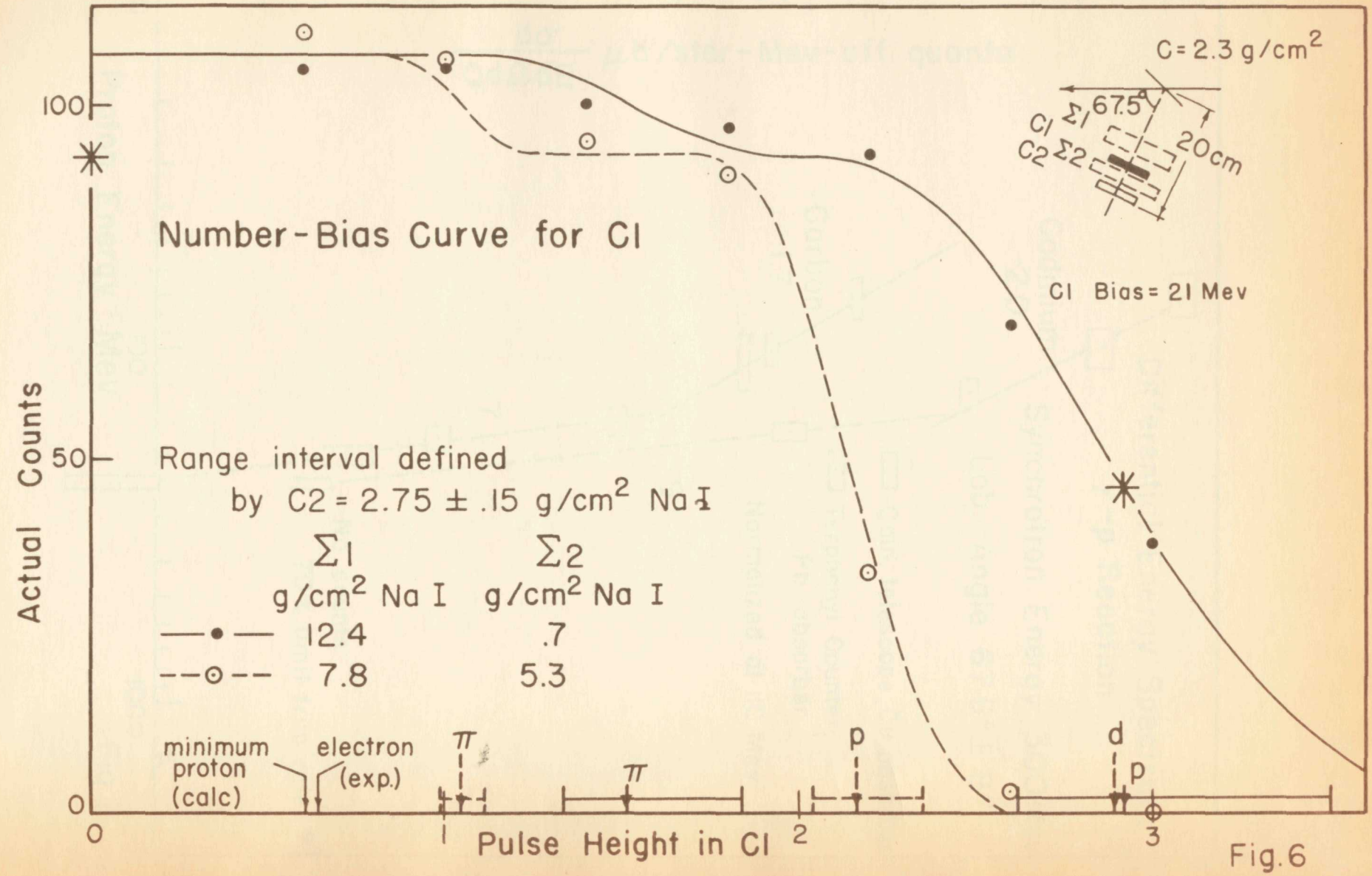
C = 2.3 g/cm²
67.5°
Σ1
C1
C2
Σ2
20cm
Number-Bias Curve for C1
C1 Bias = 21 Mev
Actual Counts
100
50
0
Range interval defined
by C2 = 2.75 ± .15 g/cm² NaI
Σ1
g/cm² Na I
Σ2
g/cm² Na I
12.4
.7
7.8
5.3
minimum proton (calc)
electron (exp.)
π
π
p
d
p
0
1
2
3
Pulse Height in C1

Fig. 6

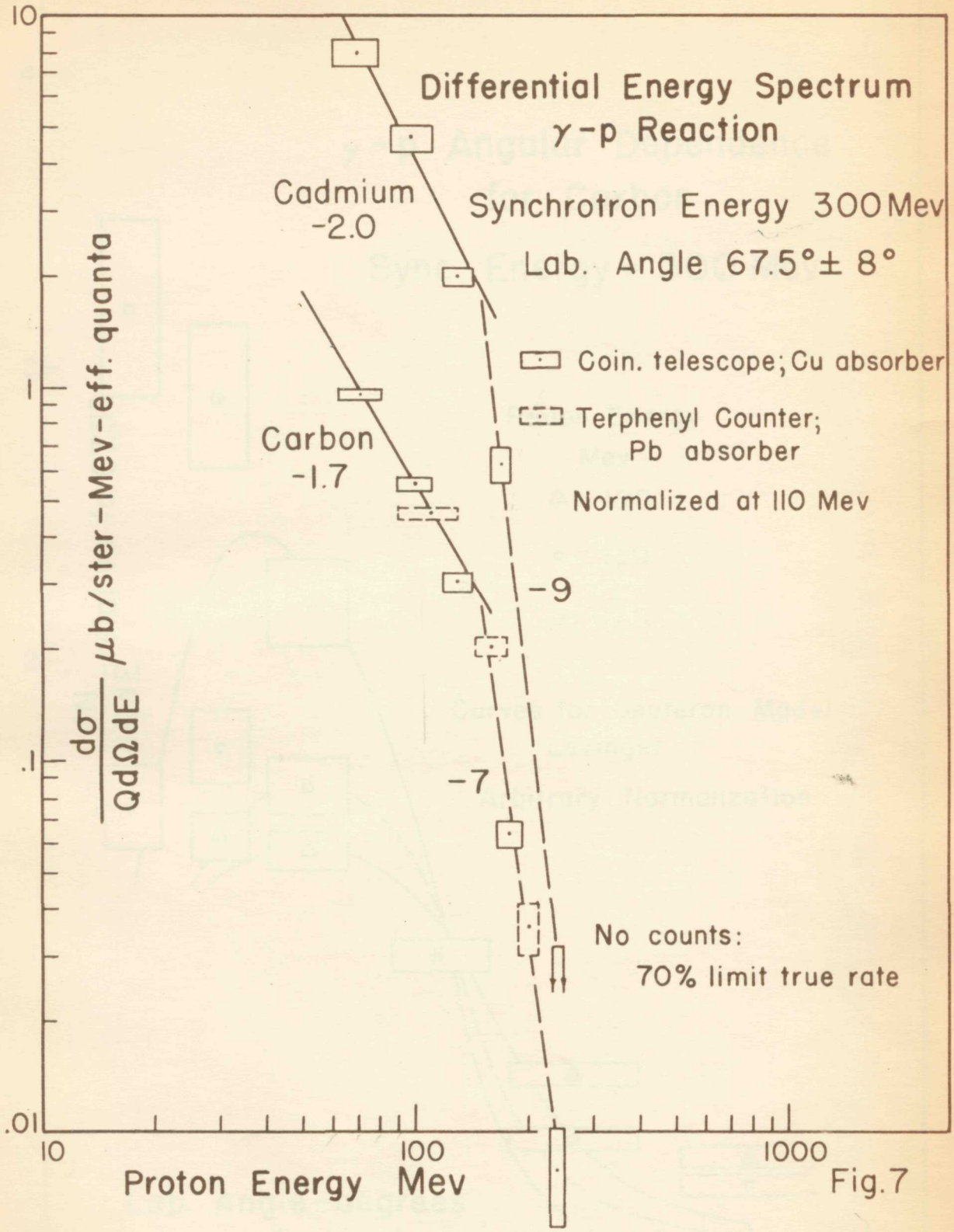
Differential Energy Spectrum
γ-p Reaction
Synchrotron Energy 300 Mev
Lab. Angle 67.5° ± 8°
Cadmium
-2.0
Carbon
-1.7
Coin. telescope; Cu absorber
Terphenyl Counter;
Pb absorber
Normalized at 110 Mev
-9
-7
No counts:
70% limit true rate
10
1
.1
.01
10
100
1000
Proton Energy Mev
dσ/QdΩdE μb/ster-Mev-eff. quanta

Fig.7

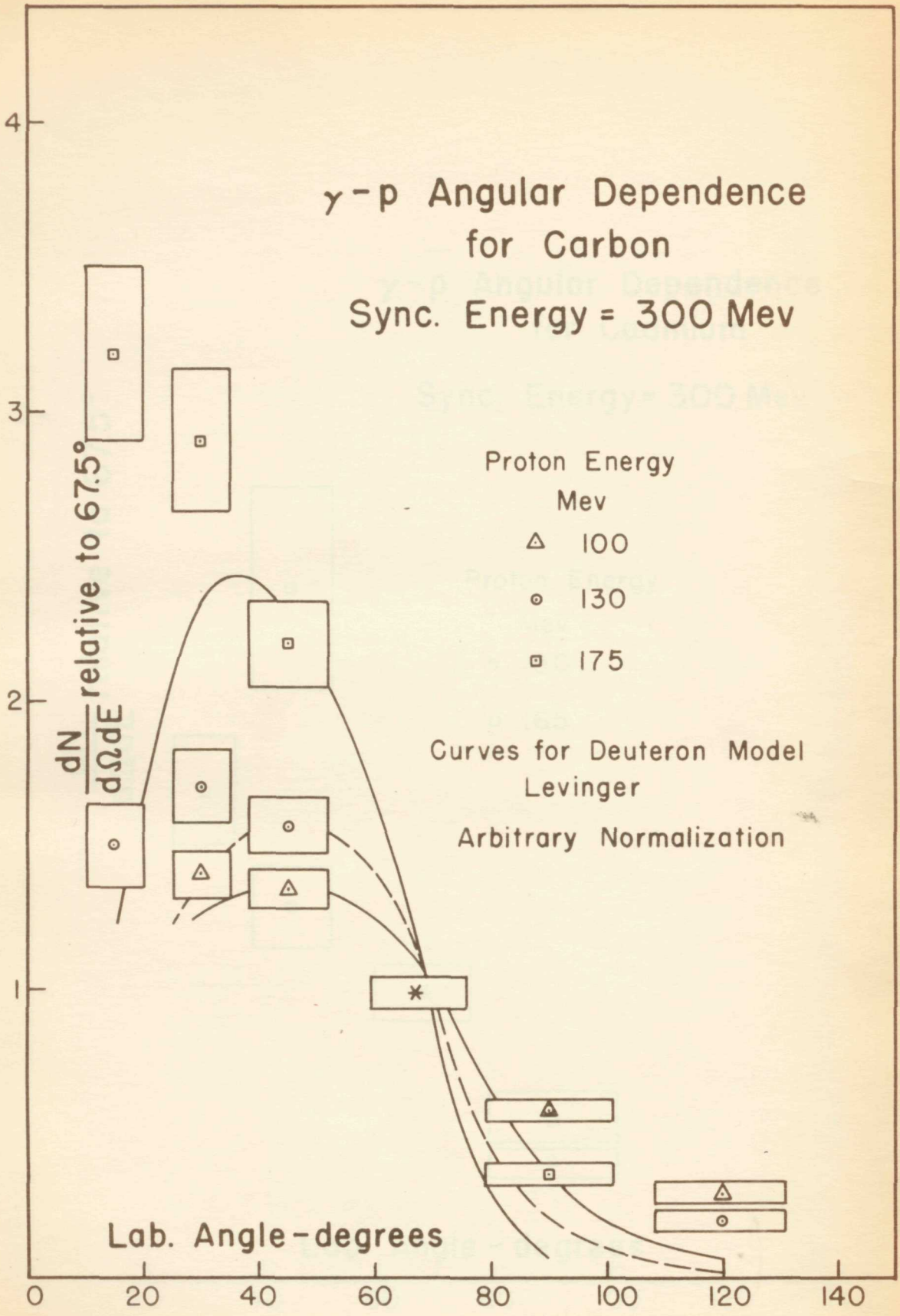
γ-p Angular Dependence
for Carbon
Sync. Energy = 300 Mev
Proton Energy
Mev
△ 100
⊙ 130
⊡ 175
Curves for Deuteron Model
Levinger
Arbitrary Normalization
dN/dΩdE relative to 67.5°
Lab. Angle-degrees
0
20
40
60
80
100
120
140
1
2
3
4

Fig. 8

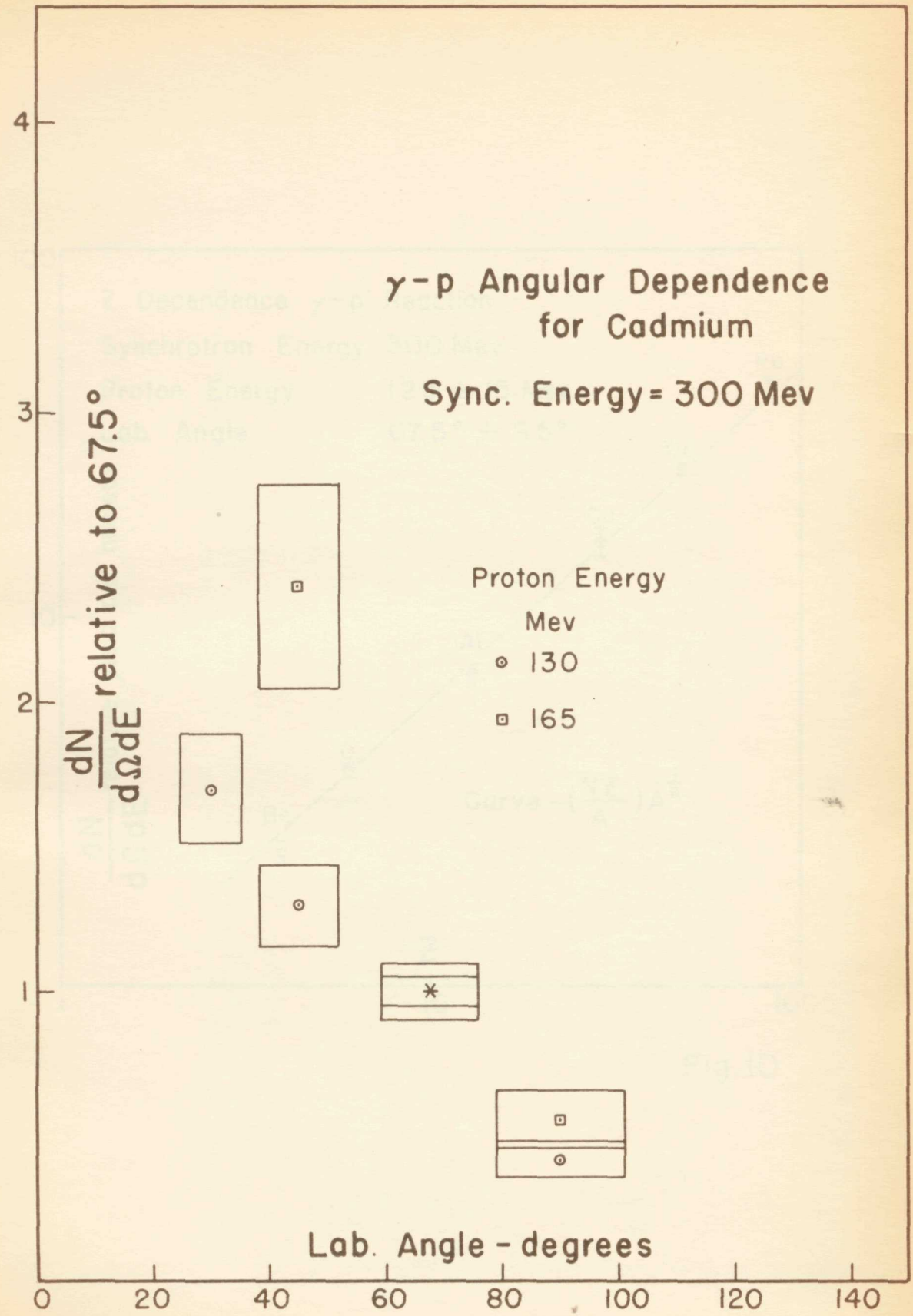
γ-p Angular Dependence
for Cadmium
Sync. Energy = 300 Mev
Proton Energy
Mev
130
165
dN/dΩdE relative to 67.5°
Lab. Angle - degrees
0
20
40
60
80
100
120
140
1
2
3
4

Fig. 9

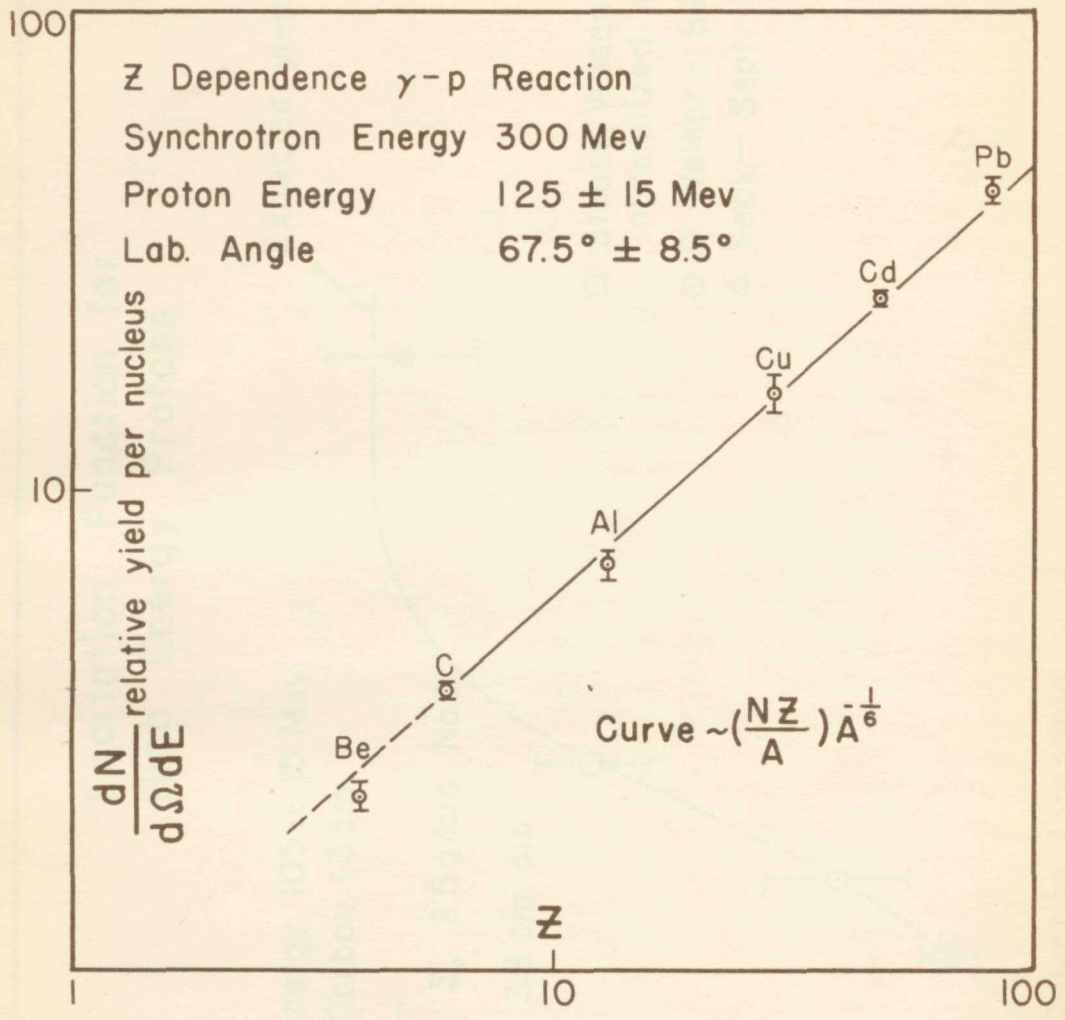
Z Dependence γ-p Reaction
Synchrotron Energy 300 Mev
Proton Energy 125 ± 15 Mev
Lab. Angle 67.5° ± 8.5°
dN/dΩdE relative yield per nucleus
Curve ~(NZ/A) A^-1/6
Be
C
Al
Cu
Cd
Pb
Z
100
10
1
10
100

Fig. 10

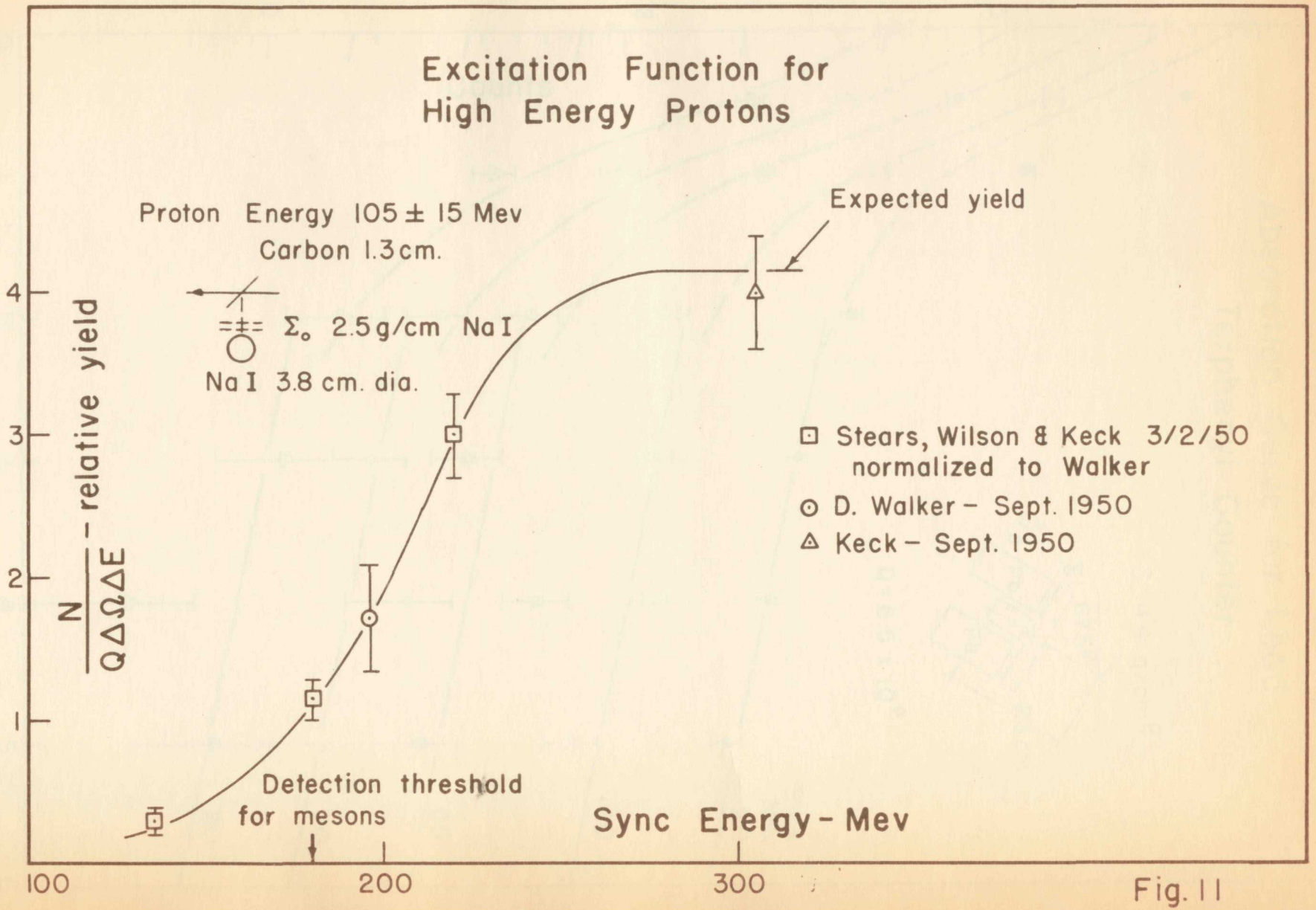
Excitation Function for
High Energy Protons
Proton Energy 105 ± 15 Mev
Carbon 1.3 cm.
Σ₀ 2.5 g/cm NaI
NaI 3.8 cm. dia.
Expected yield
Stears, Wilson & Keck 3/2/50
normalized to Walker
D. Walker – Sept. 1950
Keck – Sept. 1950
N / QΔΩΔE – relative yield
Detection threshold
for mesons
Sync Energy - Mev
1
2
3
4
100
200
300

Fig. 11

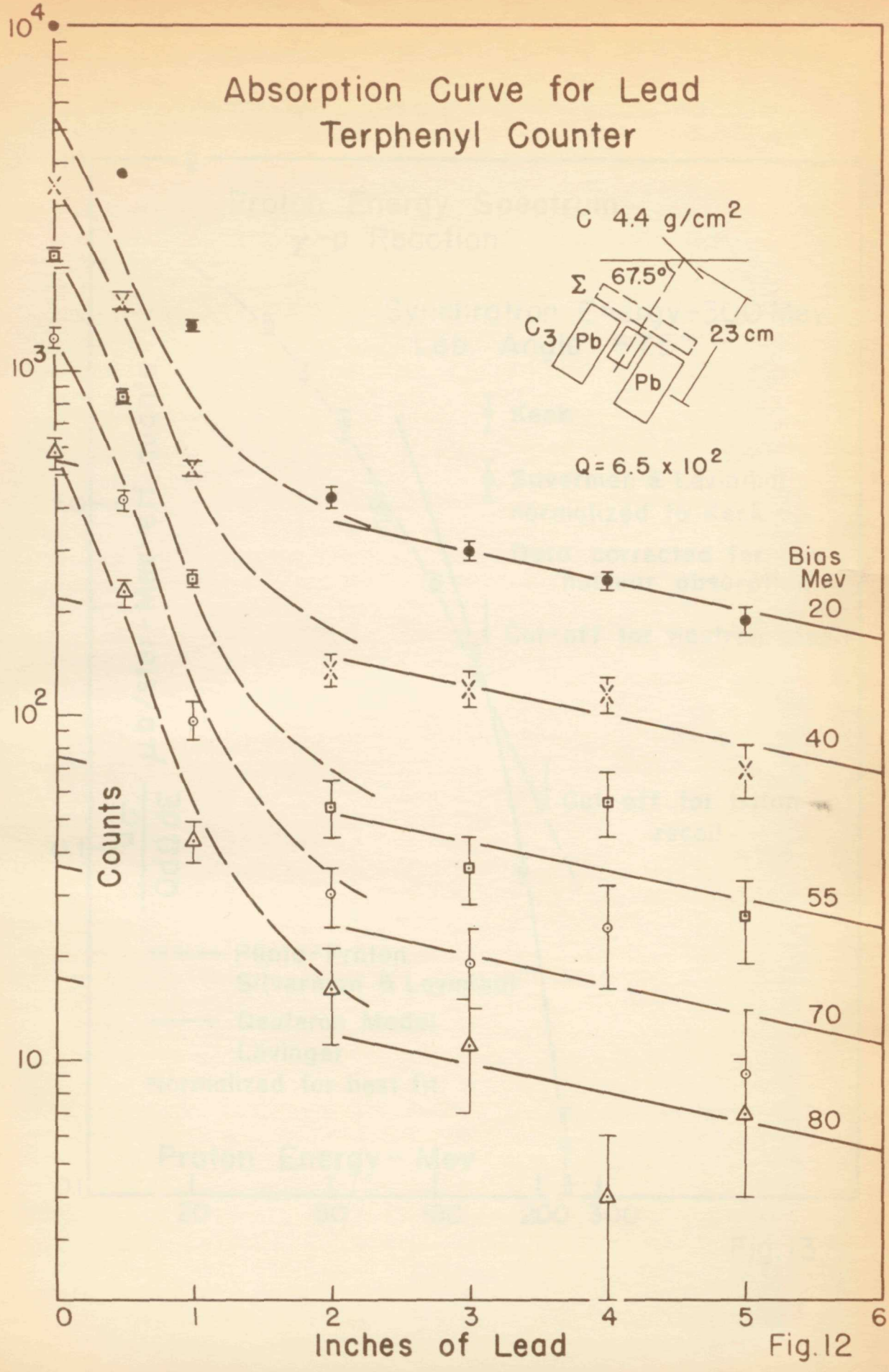
Absorption Curve for Lead
Terphenyl Counter
C 4.4 g/cm²
Σ
67.5°
C3
Pb
Pb
23 cm
Q = 6.5 x 10²
Bias
Mev
20
40
55
70
80
Counts
10⁴
10³
10²
10
0
1
2
3
4
5
6
Inches of Lead

Fig. 12

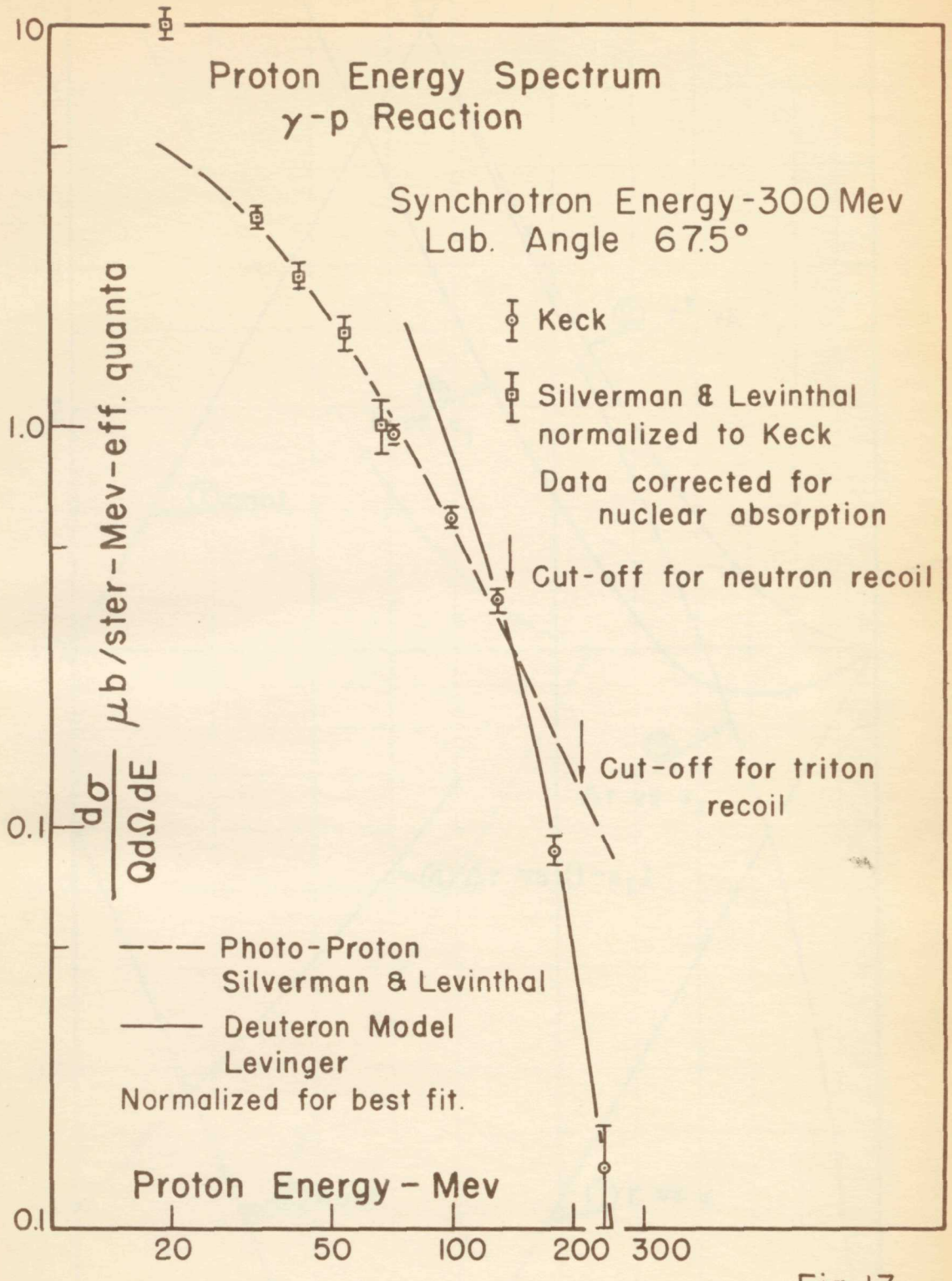
Proton Energy Spectrum
γ-p Reaction
Synchrotron Energy-300 Mev
Lab. Angle 67.5°
Keck
Silverman & Levinthal
normalized to Keck
Data corrected for
nuclear absorption
Cut-off for neutron recoil
Cut-off for triton
recoil
μb/ster-Mev-eff. quanta
dσ/QdΩdE
Photo-Proton
Silverman & Levinthal
Deuteron Model
Levinger
Normalized for best fit.
Proton Energy - Mev
10
1.0
0.1
0.1
20
50
100
200
300

Fig. 13

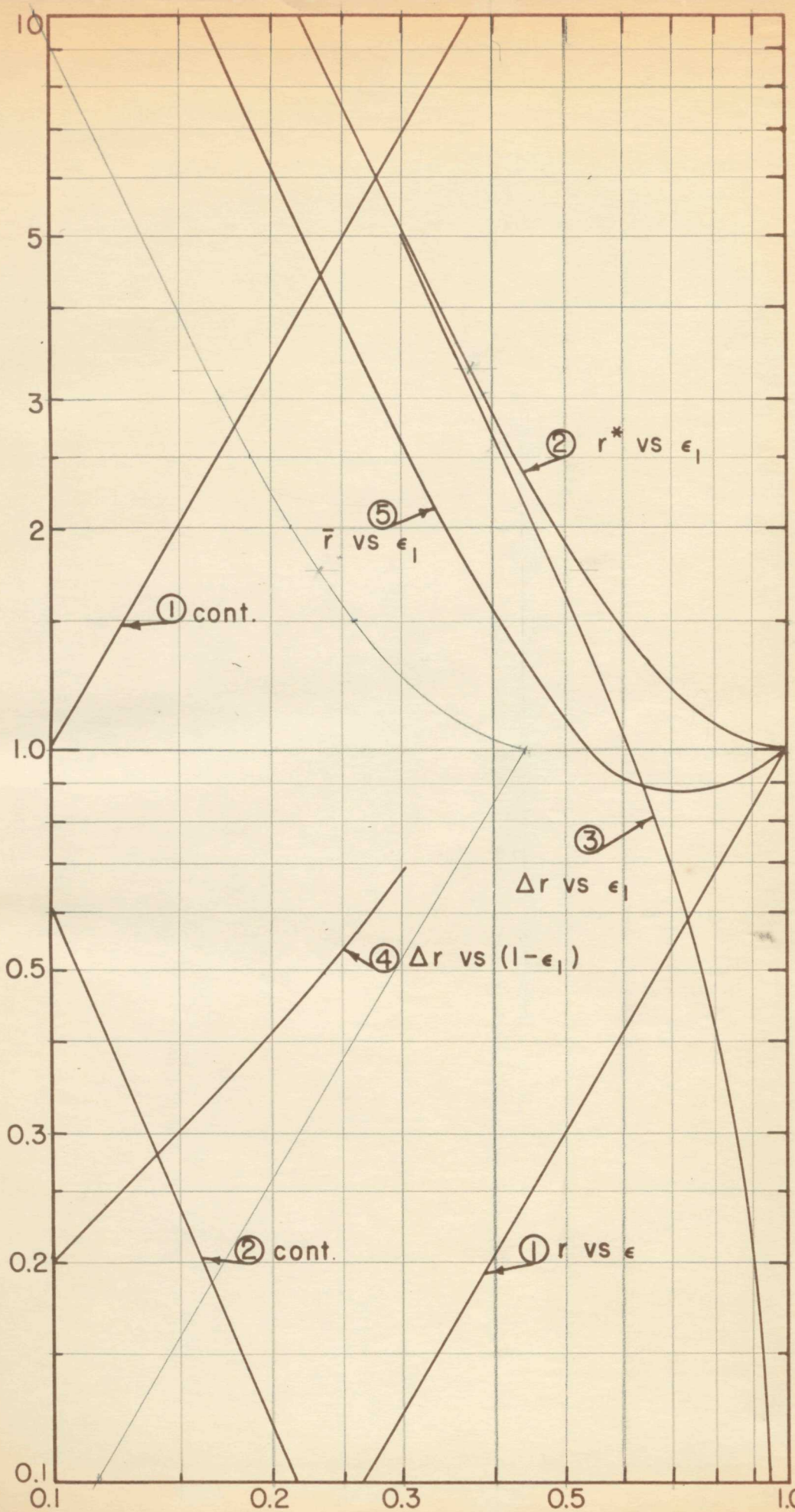
10
5
3
2
1.0
0.5
0.3
0.2
0.1
0.1
0.2
0.3
0.5
1.0
② r* vs ε1
⑤ r̄ vs ε1
① cont.
③ Δr vs ε1
④ Δr vs (1−ε1)
② cont.
① r vs ε

Fig. 14